Determination of Low Density Polyethylene Water Permeability, Transport Activation Energy and Mechanical Properties after Thermal Oxidation and Immersion in Water

A Thesis
SUBMITTED TO THE FACULTY OF THE
UNIVERSITY OF MINNESOTA DULUTH
BY

NOUMON MUNIR

IN PARTIAL FULFILLMENT OF THE REQUIREMENTS
FOR THE DEGREE OF
MASTERS IN SCIENCE IN CHEMICAL ENGINEERING

Advisors: Dr. Brian Hinderliter and Dr. Elizabeth Hill (former)
Co-advisor: Dr. Keith Lodge

August 2019

Abstract

To understand the mechanism of the degradation of plastics under environmental conditions, thermal oxidation of low density polyethylene (LDPE) thin film from a single manufacturer was studied in oxygen gas overpressure and water. Sheet polypropylene (PP) and high-density polyethylene (HDPE) as well as injection molded HDPE, HDPP, and LDPE dogbones were also studied. Oxidation of the films was carried out using a Parr Instruments pressure vessel with control at four temperatures 22, 50, 70 and 80°C with oxygen pressures of 30 and 50psi. Initial study of the immersion of LDPE films was done in a deionized (D.I.) water environment at 80°C and 50psi oxygen pressure. Permeation cup tests were done to determine the permeability of water vapor across these LDPE films at 60, 70, and 90°C. The extent of oxidation was monitored using ATR-FTIR and calculated from peak integrations. Bands that were present were carbonyl stretches (C=O), C-O stretches, and O-H stretches and were consistent with previous work on polyethylene-oxygen reaction pathways. The permeability of water vapor across the LDPE films and carbonyl content increased with temperature, oxidation time, and oxygen pressure. We postulate that the observed increase to the result of the semi-crystalline structure of the film where the amorphous regions within are more permeable to water. TGA results under nitrogen and then oxygen environments show that lower molecular weight molecules get lost first at lower temperatures and at higher temperatures there is a secondary weight loss. The dogbones were studied in the Parr vessel under 70°C and 30 psi initial oxygen pressure. There was initial change in the UTS, modulus of elasticity, and elongation at UTS; and then stabilized indicating little change and was within experimental uncertainty. This may be related to the dogbone thickness compared to the films. This study provides data for determining a reliable model for the lifetime prediction of medium-level power cables in nuclear power plants (NPPs).

Acknowledgments

Throughout my graduate school journey, there are a few groups of people I would like to thank that have helped me along the way. First and foremost, I would like to thank Dr. Elizabeth Hill for accepting me into the research group and to help initially develop the direction for my thesis work. From developing research questions to initial literature research and everything in between, it was all vital in order to move in the right direction with my work.

Secondly, I would like to give the utmost appreciation to Dr. Keith Lodge for bringing me under his guidance and has provided me with help in specific experimental setups, calculations as well which ASTM to look at, and with help on better technical writing. Related to targeted literature searches, Dr. Lodge was able to provide articles that would help better understand previous work that was done and what to expect when I was doing my research. These would provide the motivation to delve deeper into my research. Dr. Lodge has also given a lot of effort in making sure that the thesis is as complete as it can be.

Thirdly, I would like to give a huge acknowledgement to Dr. Brian Hinderliter for supporting my graduate research journey in many aspects which together made my experience a challenge that drove me to work very hard. Dr. Hinderliter was able to fund my summer research studies as well as the research I was doing during the school year. Also, when it came to the funding of additional lab supplies or equipment parts, Dr. Hinderliter was there to provide the necessary assistance in order to progress with the research. Dr. Hinderliter was available to discuss questions about the research that was going on at the time and provided good explanations and questions that helped guide my research work. Because of Dr. Hinderliter, I was able to submit my research paper for a poster at a conference.

Next, I'd like to thank the professors that are at the meetings specifically Dr. Melissa Maurer-Jones, Dr. Keith Lodge, and Dr. Brian Hinderliter for leading the discussion of our research results and what items we should consider for future experiments. Also, they all have collectively provided deadlines appropriate for our research to keep us on track. They all have collectively provided insightful comments on the paper drafts for the conference the thesis. Also, they all have graciously gave me

access to their lab equipment and lab space for my experimental preparation, setup, and analysis of my results.

There were many students I have been in contact with students in my group that helped me a lot in the beginning to get my equipment to work and with analysis of my oxidation study samples. Firstly, Daniel Zoltek really helped me analyze my FTIR results with IGOR in terms of what bands should be seen. He was available to answer questions I had, or he could put me in the right direction. Next, Adam Finke and Isaiah Salinas really helped a lot with my mechanical properties analysis of my dogbone samples in the tensile tester. Isaiah Salinas was able to develop a MATLAB code to take the tensile test raw results and turn them into useful data that I could plot for my thesis work. It cut hours of analysis I would have to do myself.

This project could not have been done without our collaboration with Dr. Robert Duckworth at Oakridge National Laboratory (ORNL). This work was supported in part by the DOE Office of Nuclear Energy NEUP award DE-NE0008540. This manuscript has been co-authored by UT-Battelle, LLC, under contract DE-AC05-00OR22725 with the US Department of Energy (DOE). The US government retains and the publisher, by accepting the article for publication, acknowledges that the US government retains a nonexclusive, paid-up, irrevocable, worldwide license to publish or reproduce the published form of this manuscript, or allow others to do so, for US government purposes. DOE will provide public access to these results of federally sponsored research in accordance with the DOE Public Access Plan (http://energy.gov/downloads/doe-public-access-plan).

On a personal note, I cannot thank my family enough for their support and really believing in me that I could succeed with my graduate school work that I was doing at the university. They have supported me in many ways while I was studying at the University whether it was financial, personal connection, or advice on how to make my graduate school experience the most beneficial that it could be. They are the core of my being and drive me to be the best that I can be as a person.

List of Figures

List of Tables

\

Table of Contents

CHAPTER 1

1.1 Historical Notes on Nuclear Power Plant Cables

The most common causes of medium voltage electrical cable failures are manufacturing defects and a variety of environmental conditions in a nuclear power plant (NPP) [1]. As the length of service of the cables increases, it is more likely for the cables to degrade and eventually fail. Other causes of accelerated degradation include radiation, overheating, water treeing, high-voltage stress, and entrance of moisture. Cable failures have resulted in plant downtime and shutdowns, and loss of safety redundancy [1]. Figure 1.1 shows the causes for cable failures and it can be seen that moisture and general aging/degradation are the dominant occurrences [1]. This is because the moisture present in the environment can infiltrate the layers of the cable and lead to a condition the central conductor produces an electric field above the dielectric breakdown of polymer insulation. Another cause worth designing experiments around are general or age-related degradation which is likely a combination of oxidation, electrical voltage, and moisture stresses.

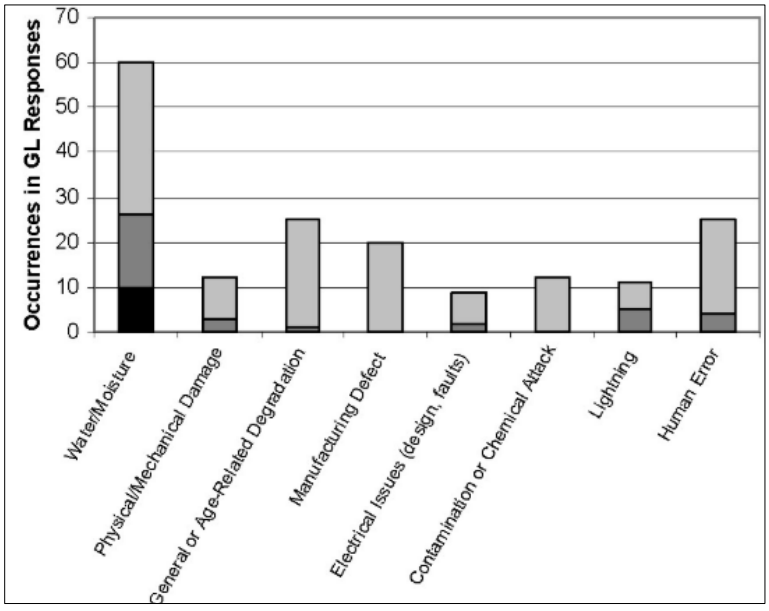

Fig 1.1: Cable failures that have occurred and the amount of times it has occurred given by Generic Letter (GL) Report in 2007 from Nuclear Regulatory Commission(NRC) [1]. The shades of gray represent the relative possibility of it occurring with black being possible causes and the lightest gray being definitive causes.

To get a sense of the lifetimes that are currently achieved, Figure 1.2 shows the service lifetime of the NPP cables which peaked around 17-27 years. This is a challenge as NPPs are relicensing, so it would be beneficial to extend the plant lifetimes 30 years and beyond.

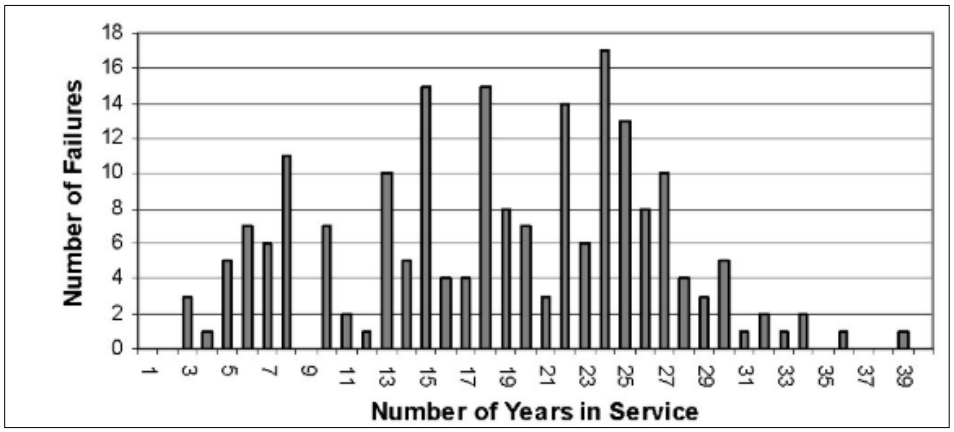

Fig 1.2: Service life of Nuclear Power Plant (NPP) cables in years from the Generic Letter 2007-01 Summary Report [1]. This does not include the replacement as normal service.

There are a few ratings of NPP cables which are: low, medium, and high voltage. Generally, low-voltage cables have ratings below 2 kV and generally operate at voltages of 525 V alternating current and below or 250 V direct current and below [1]. Medium-voltage cables are rated at 5 to 15 kV and operate at specific voltages between 4.16 to 13.8 kV [1]. Older plants have run 4.16 kV cable systems, while newer plants run at 4.16 kV and 12 kV or 13.8 kV systems [1].

Insulation materials can be thermoplastics which are lightly cross-linked during fabrication. The insulation commonly used in low and medium voltage cables are cross-linked polyethylenes (XLPEs) and ethylene propylene rubbers (EPRs). For low-voltage cables, most XLPEs were made with flame retardant additives, and EPRs can also be manufactured with flame retardants because of the low operating temperature. Most U.S. NPPs use EPR insulated medium-voltage cables, although a few cables are insulated with XLPE. Fig 1.3 shows the layers of NPP medium voltage cables. The conducting layer is typically copper metal that can be bundled in variety of ways. There are also shielding layers, which are typically conducting tape or extruded polymers, are used to increase the uniformity of the voltage stress and contain the electric field within the insulation. Then

finally there is an outermost jacketing layer which is often 2-chlorobuta−1,3-diene (Neoprene) polymer.

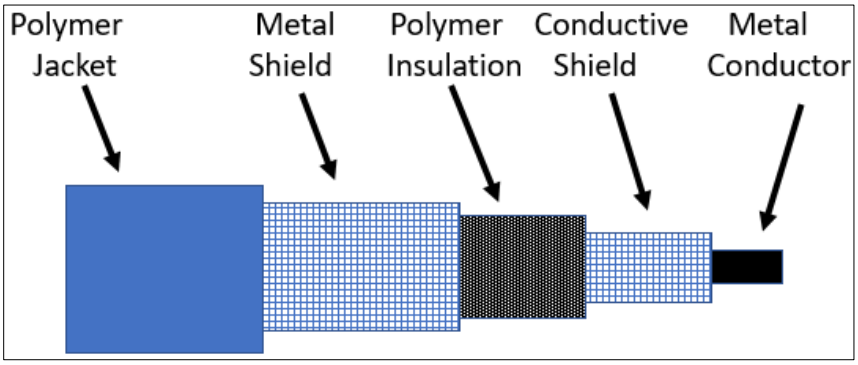

Fig 1.3: Diagram of a typical NPP power cable and its layers [2].

1.2 Qualification/Monitoring of Cable Insulation Techniques

Low and medium voltage cables are qualified by the Condition Based Qualification(CBQ) that uses testing techniques to monitor the degradation [1]. These testing procedures measure and record the level of cable degradation in chemical, electrical and/or mechanical properties to determine the shape of the degradation property vs. aging time of the cable being tested. The downside is that the testing can only tell about a localized part of the cable, not the whole cable [1]. All of them is summarized in a table in chapter 1.4.

An important thing to note is that EPRs exhibit “induction-time” behavior, where the testing technique might show little indication in aging until a dramatic change occurs just before failure. This may be caused by flaws present in the processing [1]. High-temperature polymers can be affected by extrusion equipment, tooling, and processing. In some medium-voltage cables, the cleanliness, smoothness of extrusion, and type of cure system are thought to affect long-term performance. All the monitoring techniques that are used can be categorized as techniques that either require removal of sample or do not require removal of sample. The techniques below are techniques that require removing samples from the cable.

The elongation at break of a polymer-based cable insulation is done under a tensile test and is the benchmark physical property that assesses the structural integrity using the absolute elongation at break, which is the absolute strain a sample of the

material before breaking. It can also be used to observe the degree of ductility of that material as a result of aging. For EPR cables, they are required to be between 70% to 230% and XLPE between 70% and 310%, depending on formulation [3]. IEEE standards (such as IEEE 323-2003) for elongation at break as a condition monitoring technique. EPRs experience induction-time behavior and one example of this is when elongation strain % is done against aging time and it results in a small change followed by a substantial drop from 150% to 0% for EPR [2].

The next technique is oxidation induction. In most polymers, radiation and thermal degradation are accompanied by oxidation when in the presence of oxygen. During exposure to radiation and thermal aging conditions, antioxidants, added during formulation in the polymer cable insulation, can act as free radical absorbers and are consumed at a rate defined how severe the degradation is [2]. After antioxidants have been consumed, the polymer usually begins to degrade more rapidly [2]. Polymer properties known as oxidation induction time (OIT) and oxidation induction temperature (OITP) can be determined on standard differential scanning calorimetry (DSC) instruments [2]. Micro-samples (about 10 mg) can be used, and their properties are dependent on the remaining levels of antioxidants and the extent of oxidation (or degradation).

Varying the amount of polyethylene present in the EPR insulation cable formulation determines the degree of crystallinity for the EPR. The cable insulation was thermally aged, and the DSC was run from 0−180ºC at a rate 5ºC/min under Ar-gas [1-2]. Combined environment aging was done at 80ºC and it increased the peak from 50ºC to 100ºC and aging at 22ºC led to a DSC peak at ~45ºC [4]. As with EPR, many formulations exist for XLPE as well which results in varied results from testing. Majority of the unaged XLPE insulations have a peak around 90ºC and then the main melting peak at ~120ºC [2].

Thermal gravimetric analysis (TGA) is carried out using commercially available thermal analysis instruments and requires sample sizes similar to those used for OIT/OITP. TGA testing is usually carried out as an alternative to OIT/OITP on samples because the sample chambers in TGA equipment are chemically far more robust than those used in DSC [1,5]. A typical TGA trace consists of a plot of sample mass loss

against temperature. J. Boguski *et al.*, did TGA testing on ethylene vinyl-acetate copolymer (EVA) as the jacket of cable along with mechanical testing and IR spectroscopy [6]. The jacketed cables did have XLPE and EPR samples as cable insulation. Using a thermograph, it was shown that increasing the radiation dose from 0 to 1.4 MGy at a rate of 6 kGy/hr at isothermal 400ºC in air flow lead to delay in weight loss because of the longer times of thermal decomposition [6].

Gel fraction and solvent uptake revolves around competition of cross-linking and chain scission that usually define the level of aging in a polymer. Micro-scale(~1mg) samples are used like oxidation induction testing. Gel fraction increase means that crosslinking dominates, and solvent uptake factor increase means chain scission dominates. This can be shown to correlate with structural integrity and elongation at break. Tadao Seguchi *et al.*, have done experiments on gel fraction and swell-ratio. EPR and polyethylene film samples were cross-linked by gamma-radiation under a vacuum at room temperature and gel fraction was plotted against dose rate. What was found was, given a fixed film thickness of 1mm and dose rate of 0.5 MGy/hr, the yield of the gel was hardly affected [7]. Swelling ratio was also plotted versus the radiation doses under vacuum and was found to decrease with the dose [7]. Another separate study was done by Tadao Seguchi *et al.* showed that gel fraction and swell ratio data when plotted with film thickness was concave up and down trend respectively for EPR [8].

The most basic, defined, and well-established testing technique is the determination of the density. When polymers are exposed to air, oxidation dominates the degradation processes if crystallinity stays constant. The resulting oxidation products in the polymer lead to an increase in density. The greater the degree of aging, the larger the concentration of oxidation products and the higher the density. This provides a useful means of evaluating the degree of polymer aging. The density of small samples, ~1mg, of polymer can be measured. Radiation exposure of 0.0175 Mrad/hr (175 Gy/hr) at 43ºC in air and an increase of radiation resulted in increase in density [9]. This correlated well with the elongation at break, which decreases with increasing density [9].

Modulus profiling (indentation testing) measures how the modulus varies across the cross section of a material [1]. In modulus profiling, the sample polymer sample is indented with a parabolic tip [12]. The force applied is known so the inverse tensile

compliance can be calculated which is closely related to the modulus [12]. The modulus tends to increase with aging under thermal and radiation aging conditions. The modulus profiling technique allows a correlation to be made between modulus measurements and elongation results. It has been found to be useful for observing the aging of EPR insulations. For unaged EPR, the degree of crystallization yields different modulus values from 4-60 MPa based on 3 samples [12]. Aging the EPR results in a slow increase in the modulus from zero time until before the induction-time takes into effect where there is a drastic increase after the induction time. Therefore, the modulus profile is relatively insensitive to degradation for EPR insulation materials until the induction-time region is approached [12].

The last technique is Fourier Transform Infrared Spectroscopy (FTIR) analysis which utilizes the changes in structure that occur result in the formation of new chemical bonds, which have absorption characteristics that are different from the bonds in the original unaged material. The dominant oxidation mechanisms for polymers aged in air produce carbonyl species, which absorb IR light at characteristic wavelength (around 1720 cm^{-1}). So, the amount of degradation in a polymer can be inferred from the ratio of absorbance at ~1,720 cm^{-1} to ~1300-1400 cm^{-1} which will give a measurement of the oxidation levels [8,11]. The FTIR analysis is limited to thin samples as thicker samples absorb all incident light.

1.3 Electrical Property Testing Techniques for Qualification

The next category of techniques are based on electrical functionality which can reveal degradation information in cable insulations. The advantage of electrical techniques is that they can be used in NPPs and possess remote-testing capability. They can often reveal problems along the whole length of a cable [1]. They are most useful in identifying and locating problems in cable systems in plant and confirming cable performance. This is opposite of the previous testing techniques as they limited to providing data at the localized point where the test is performed.

The first technique is Partial Discharge (PD). PDs are electrical discharges that occur in gaseous voids that can occur in solid insulation materials [1]. During testing in which the voltage is slowly raised, the voltage at which PDs are observed in each cycle is known as the PD inception voltage. Decreases in the PD inception voltage are an

indication of significant degradation of the insulation material. The PD test is potentially damaging since the discharges can induce insulation degradation over a period of time due to localized overheating. One study looked at partial discharges of 15 kV XLPE and EPR cable insulation and the AC breakdown voltages [13]. The cable insulation tested were 15 kV XLPE and EPR cable samples which were determined after the accelerated aging. In the experiment, the AC breakdown was evaluated after the application of up to 10,000 switching impulses [13]. The results showed that the tested XLPE samples showed 55.2% of the original PD inception voltages while the value for the EPR cable samples was 60.9%, [13] which indicates a decrease in PD inception voltage. For the XLPE cable samples aged by 10,000 impulses, the AC breakdown voltages were reduced by 9.8% [13] while the EPR cable samples decreased by 33.9% [13]. Some possible explanations for this is imperfections in the cables' insulation layer due to manufacturing such as the cross-link byproduct, moisture, and foreign objects [13]. The PD test has limitations for use in the field since it requires relatively high voltages to be applied to the cable, which would be a concern due to the potential to damage the cable or surrounding equipment. The PD test is typically performed on medium-voltage cables and not on low voltage cables [1].

The next technique is Frequency Domain Reflectometry (FDR), which is a nondestructive cable-testing technique based on transmission line theory [1]. The FDR technique uses a sweeping frequency signal to transmit through an electrical cable circuit and analyzes the circuit impedance changes that are reflected. The reflected signals are measured in the frequency domain and then converted into the time domain using an inverse Fourier transform [1]. The FDR method generally requires a comparison with a baseline measurement to identify anomalies along the conductor or insulation material. FDR methods include line resonance analysis (LIRA) and frequency time domain reflectometry (FTDR) [14]. Both of these techniques can be used for low voltage cable insulation materials. LIRA is an electrical test which a high frequency white noise, low energy electrical signal is applied to the cable [15]. Evaluation of the modulated signal for amplitude and phase differences of the frequency dependent resonances can detect impedance changes along the entire length of cable [15]. Bulk damage, as well as localized damage and age-related degraded segments are able to be detected and located

by the resonances [15]. LIRA has a big advantage in that it allows for diagnosis of cables that are difficult to access. FTDR is a non-destructive test that, given the distance, sends direct current pulsating signals and measures the reflection to locate changes in impedance [14]. Both can be used to determine the degradation severity, for both thermal and mechanical degradation/damage. This is an area of on-going research and evaluation.

An electrical property that can be measured is dissipation factor. Testing technique for cable qualification that has been studied with some success has been the measurement of the dielectric loss tangent (or dissipation factor tan δ) for shielded medium-voltage cable insulation [1]. Tan δ is a dimensionless property of a dielectric, which is determined by the insulator's structure. Therefore, changes in structure brought about by aging results in changes in tan δ. A study by G. Bader *et al*., tested medium voltage cables (5-35 kV) with XLPE insulation from widely spaced geographic locations around the United States. A series of laboratory experiments were done on cable models aged at 8 kHz frequency to an average voltage stress of 85 V/mil while immersed in tap water at 75°C for 40 days [16]. The result was voltages ranging from 7.6−12kV depending on the location and dissipation factors(100 tan δ) from 0.005 to 0.069 [16]. Another parameter that can be plotted is the power factor as a function of aging of the XLPE and EPR insulation. The aging was simulated for 20, 40, 60 years of service life and what was found was that there is a consistent increase in the power factor as aging increased. This proves that this can be used to monitor the condition of the insulation cables[17].

1.4 Cable Insulation Qualification Summary

Chapters 1.2 and 1.3 discuss a plethora of qualification techniques and approaches in determining when the cable insulation is at risk of failure, what extent degradation has occurred, and possibly where that is occurring. Each of these has its own advantages and limitations and the application of a certain technique is very industry situation dependent [1]. Therefore, it is possible that not all of them are used together to evaluate the cable insulation. Also, what the service environment of the cable prior to detection in degradation is important and that will dictate what qualification tests are necessary [1]. Below shows the summary of the qualification methods of the medium voltage cables.

Table 1.1: Summary description of the cable techniques and approaches as well as their advantages and limitations. The type of technique is mentioned, electrical, mechanical, or chemical, in bold parenthesis.

Method	Description	Advantages	Limitations
Elongation at Break **(Mechanical)**	• Measures strain of sample prior to breaking	• Provides trend worthy data amongst cable insulation materials	• Requires access of the sample to test
Oxidation Induction Time w/ DSC or TGA **(Chemical)**	• Measures the thermal stability in an oxidation environment	• Provides information about cable insulation and only small samples required	• Requires access of the sample to test
Gel Fraction **(Chemical)**	• Measures the extent of crosslinking in material	• Can get good insight in extent of degradation	• Need experience to get best results
Density **(Chemical)**	• Measures by the mass over the volume	• Can be correlated with electrical properties	• Requires access of the sample to test
Modulus Profiling **(Mechanical)**	• Measures the changes in modulus using an indent tip	• Provides trend worthy data amongst cable materials	• Requires access of the sample to test
FTIR **(Chemical)**	• Measures changes in chemical structure using its absorption.	• Only small samples required	• Surface level analysis
Partial Discharge **(Electrical)**	• Measures the partial electrical discharges	• Access to cable not required and can be compared to other cable insulation materials	• Potentially destructive to the sample
FDR **(Electrical)**	• Analyzes the changes in electrical impedances using a sweeping frequency signal	• Non-destructive and useful in locating defects	• Have to find the right cable to do test

Dissipation Factor **(Electrical)**	• Measures degradation of dielectric properties	• Easy to perform to get trend data and access to cable not required	• Have to find the right cable to do test

1.5 Drawbacks from Cable Qualification

Given that oxidation is one of the dominant degradation mechanism, this leads to the discussion of Diffusion-Limited Oxidation (DLO) phenomena. This occurs at highly accelerated aging conditions such as very high radiation dose rates[~5 kGy/h (0.5 Mrad/h)] and/or very high aging temperatures(150 °C). Under these high aging conditions, the oxidation rate in the oxidized polymer is much faster than the supply of the oxygen from the surrounding air atmosphere. This leads to significant drops in dissolved oxygen concentration, almost to zero. This significantly reduces the oxidation reaction in the inside of the polymer cable insulation. As a result, DLO may overestimate cable insulation lifetimes [1]. This occurs because the oxidation will progress is sufficiently slow for oxygen to diffuse into the polymer material around it. This is due to an additional oxidized layer created that the oxygen must diffuse through before reaching the polymer material surface and therefore limiting the oxygen diffusion. For the purpose of this thesis work, Diffusion-Limited Oxidation effects are assumed to be absent for the low-level thermal, radiation, and oxidative environments with thin samples [1].

Another limitation of all these techniques is that they evaluate the cable in the condition present during testing. Medium voltage power cables are often designed to provide current during accident conditions when there is increased humidity and/or temperature. It is quite possible to have partial or complete immersion of the power cables as well. Evaluation during normal service evolutions are not intended to test a cable that is immersed only periodically or only in accident conditions.

1.6 Thesis Statement

With the various chemical, electrical, and mechanical properties used for qualification and their corresponding studies and results, it gives a good framework to develop a path for this thesis work. Many works have looked at temperature and radiation aging and its effects but very little if any has focused on temperature in combination with

moisture and direct oxidative environment in a closed system unlike an oven. Because of this, the goal of this thesis is to look at the chemical and mechanical properties and how that is affected at elevated temperature within the range of operation of the polymer insulation materials. Quantitatively, this thesis work aims to link the chemical and mechanical properties in a way that hasn't been done much in the literature. Because of the induction time experienced in polymer insulation, it is hypothesized that elevated temperature aging will cause more extent of the oxidation.

CHAPTER 2

2.1 Concepts and Theoretical Background

As stated in the previous section, there are many factors in the environment that can affect the NPP cable insulative material such as temperature and presence moisture resulting in oxidation. To better understand these effects, different types of polymers will be introduced. Next, the theory of gas transport using permeability and diffusion will be described. Finally, the oxidation kinetics of PE will be described to better understand what products and functionality can be observed.

2.1.1 Types of Polymers and Characteristics

Gas or vapor transport through a polymer depends on the morphology of the polymer that are crystalline, semi-crystalline, and amorphous. Crystalline polymers are when the molecular backbones are mostly aligned in a crystal structure that does not allow for significant diffusion, although a fully crystalline structure is not favored for cable insulation. This is due to the brittleness resulting from high crystallinity.

Amorphous polymers can be broken up into glassy and rubbery polymers and the glass transition temperature, T_g, defines the transition point from glassy to rubbery polymer. As a result, in most cases amorphous polymer regions are more ductile. In regard to their gas and liquid transport, amorphous polymers differ significantly. Rubbery polymers follow Fick's laws of diffusion, which will be discussed in the next sections, and tend to describe the diffusion well. On the other hand, glassy polymers do not follow either of the Fick's Laws, or Non-Fickian diffusion. The complexity to describe these polymer diffusions is substantial and often the governing equations arise from free volume theory of the gasses. It states that the energy of the gas molecule is dependent on its free volume in the polymer matrix. Since these are not favorable in the context of the polymer insulation, these types of polymers will not be further discussed.

Semi-crystalline polymers will be the focus because all the polymers used for insulation material are of this type. Polyethylene and polypropylene are semi-crystalline polymers because they consist of a nearly impermeable crystalline phase and a permeable amorphous phase which dominates the gas transport. Because of these two phases present, the properties of the same polymer can vary based on the history, molecular

weight, and degree of crystallinity. Depending on the backbone of the polymer, the polymers can react differently to temperature and the aging due to the mobility of the backbone chains. As a result, the crystallinity of the polymer can change as it is thermally aging relative to the unaged counterpart. Increasing the crystallinity results in the little mobility in the chains leading to more rigid polymer.

Polyethylene, of a defined molecular weight distribution, is a semi-crystalline polymer with a T_g of −120°C, which means it has rubbery amorphous phase during operation [38]. It is in the general class of polymers called polyolefins, which are a large class of polymers that are produced from a simple monomer formula C_nH_{2n}. Polyethylene is a nonpolar polymer meaning it is hydrophobic and does not absorb nor interact with water at room temperature easily. It is used in every aspect of our daily lives like grocery bags, bottles, and pipes just to name a few. There are a few different grades of polyethylene and this relates to the packing of polymer chains, which affects the crystallinity. Also, each grade has certain degree of branching of the side chains off the main polymer chain. The grades are linear low, low, medium and high-density polyethylene. Linear low and low density polyethylene (LLDPE & LDPE) have high degree of branching therefore less crystallinity. On the other hand, high density polyethylene(HDPE) few branching chains are present, so it has higher crystallinity leading to little access for the gas molecule transport.

2.1.2 Applications of Work

Besides applications in the field assessment of NPP cable insulation and jacket materials, various other applications can be explored specifically food packaging and medical implants and devices. Plastic food packaging is prone to the passage of small gasses (CO_2, O_2, N_2, & others) and water vapor (H_2O) because of different stages of the industry process such as manufacturing, handling, packaging, and on the shelf [31,34]. The end effect is the reduction of the shelf life of the food. It was found that when it comes to the handling and packaging service, the water vapor and oxygen are the two most important gasses and when it comes to food degradation, CO_2 also becomes more important [31,34]. Table 2.1 shows these gasses and their important properties in regard to barrier properties. Another application is in the medical field such as devices and equipment (paraphernalia) such as tubing, sutures, and implants because of the rapid replacement or

use in conjunction with other materials for better biocompatibility [30,35,36]. Ultra-high molecular weight PE was found to be a great material for hip implants along with metal materials [37]. Another application is in encasement of underground piping with a thin layer of PE. The purpose of encasement with PE is to prevent the metal pipes from corrosion and is good at reducing the electrolytes present in soil in the landfills available for corrosion at the metal surface of the pipes [44].

Table 2.1: Some of the important properties of gasses concerning permeability [31].

Property	N_2	O_2	CO_2	H_2O
Molar Mass (g/mol)	28.01	31.99	44.01	18.01
Molecular Diameter (cm) $\times 10^{-8}$	3.15	2.98	3.34	2.75
Gas Density (kg/m^3)	1.25	1.43	1.98	0.804
Solubility of gasses in water at different temperatures/ (cm^3/dm^3)	16.0 (20°C)	31 (20°C)	878 (20°C)	-
	12.5 (40°C)	23 (40°C)	530 (40°C)	-
	10.2 (60°C)	19 (60°C)	360 (60°C)	-
Diffusion Coeff. of gasses in water @20°C/(cm^2/s) $\times 10^5$	1.64	1.8	1.77	-

2.2 Polyethylene Oxidation Reaction and Degradation Mechanism

To determine the effects of thermal oxidation of PE, it is necessary to look at the general oxidative reaction pathways that take place in polyethylene. This way the possible functional group products. During thermal oxidation process, the polymer chains

in the polymer become modified with different functionality groups [41,42]. As seen later in this section, this is accompanied by scission of the chain bonds, which leads to branching in the intermediates and the products [41]. It is important to note that the degree of oxidation on polymer is dependent on many factors such as: polymer backbone chain structure, % crystallinity, and super-molecular structure [42]. Therefore, it is difficult to determine the exact mechanism, so the generalized steps and products will be shown for polyethylene [42].

For general polyolefins, such as PE, the mechanism for thermal oxidation is called radical chain reaction with degenerate branching. In this mechanism, the presence of radicals formation to give functionalized end products [41]. With degenerated branching, side products can form depending on the polymer chain conformation and geometry. Intermediates that can form, which are meta-stable species that are comprised of radicals. Radicals are building blocks that will be used for later reaction steps and provide for a reaction site for the oxidation to take place.

Fig 2.1 shows the kinetic curves for molecular mass, presence of oxygen and end products and formation of intermediates(propagating radicals, hydroperoxide groups). The molecular mass of the PE will decrease because the intermediates will fragment the polymer chain and cause an increase of low molecular weight products with oxidized structures in the short term. The intermediates eventually reach a maximum because as radicals form and propagate the polymer chain causing radical-radical interaction which will cause the chain to stop or terminate. The radicals chains may react and bond with other nearby chains resulting in cross-linking and increase in molecular weight.

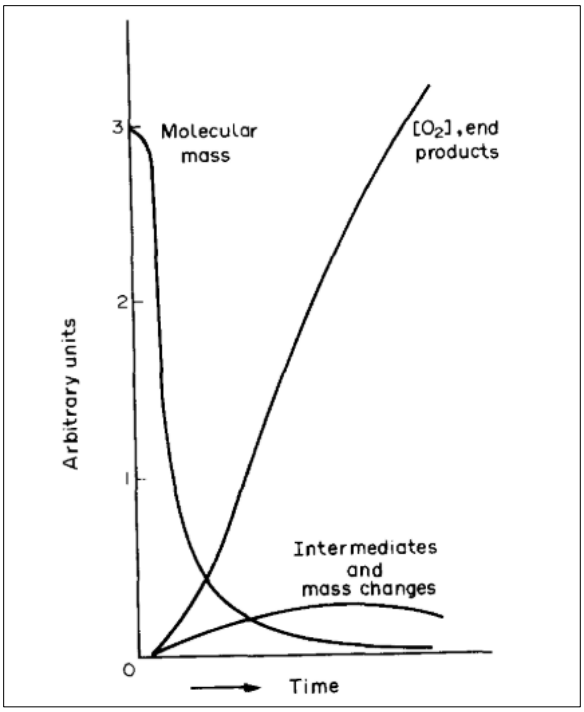

Fig 2.1: Typical sketch of the molecular mass, oxygen uptake, mass change and formation of intermediates and products for polyethylene oxidation [42].

The mechanism for polyolefin oxidation follows a general mechanism depending on the O_2 pressure [42]. The difference in mechanism between the levels of O_2 pressure is in what radicals determine the reaction and the relative reaction rates. At higher O_2 pressure, the reaction steps are faster specifically the oxidation of the radicals. Also, the peroxy, RO_2^* , radical and the reactions that involve that radical are the rate determining which helps simplify the step and see the main reactions and products[41,42]. For this study, it will be assumed that enough time of thermal oxidation has taken place and the oxygen pressure is high enough where the high O_2 pressure mechanism can be used and every macroradical, R^*, is oxidized [41].

Most of the end products from oxidation result from hydroperoxide, ROOH, decomposition processes that combine within molecular cages, group of surrounding radical and polymer chain molecules, formed by peroxy radicals and during radical termination processes [41-43]. There is also a smaller proportion of products are going to be of broad range and they are formed from radical reactions escaping the molecular cage and by active intermediate products formed by them [41]. The mechanism steps are

shown in fig 2.2 which are: initiation, radical oxidation (very fast), chain propagation, degenerated branching, and finally termination[41].

Primary Initiation:

$$\sim CH_2\sim + O_2 \rightarrow \sim \dot{C}H\sim + H\dot{O}_2 \quad (2.1)$$

$$\sim CH_2\sim + H\dot{O}_2 \rightarrow \sim \dot{C}H\sim + H_2O_2 \quad (2.2)$$

Radical formation on the polyethylene site as a result of the oxidization of an active site on the carbon atom for propagation.

Radical Oxidation:

$$\sim \dot{C}H\sim + O_2 \rightarrow \sim CH - \dot{O}_2\sim \quad (2.3)$$

As mentioned previously, under high pressure of oxygen, this step is very fast and the assumption of every macroradical, R^*, is being oxidized given the time of oxidation.

Polyethylene Hydroperoxide Formation:

$$\sim CH - \dot{O}_2\sim + \sim CH_2\sim \rightarrow \sim CH - OOH\sim + \sim \dot{C}H\sim \quad (2.4)$$

By forming the hydroperoxide, future functionality of polyethylene can be formed as a result of the decomposition of the hydroperoxide.

End Chain Radicals Formation and Chain Scission:

$$\sim CH - \dot{O}_2\sim \rightarrow \sim \dot{C} - O - OH\sim \rightarrow \sim HO - C - \dot{O}\sim \rightarrow \sim COOH + \sim \dot{C}H_2\sim \quad (2.5)$$

Hydroperoxide Decomposition:

$$\sim CH - OOH\sim \rightarrow f\sim CH - \dot{O}\sim + fH\dot{O} + (1-f)(products + H_2O) \quad (2.6)$$

In this step, oxidized structures along the polyethylene chain are formed which will cause the chain to break into fragments forming lower molecular weight products (aldehydes, carboxylic acid, ketones, etc.).

In the previous equation, the alkoxy radical, $\sim CH\dot{O}$, transforms to form chain-end radicals, which can be further broken down into chain-end radicals and react further:

$$\sim CH - \dot{O}\sim \rightarrow \sim COH(aldehyde) + \sim \dot{C}H_2(chain\ scission) \quad (2.7)$$

$$C\dot{H}_2 + O_2 \rightarrow \sim CH_2\dot{O}_2 \quad (2.8)$$

$$\sim CH_2\dot{O}_2 + \sim CH_2\sim \rightarrow \sim CH_2OOH + \sim \dot{C}H\sim \quad (2.9)$$

$$\sim CH_2OOH \rightarrow g\sim CH_2\dot{O}\sim + gH\dot{O} + (1-g)(products + H_2O) \quad (2.10)$$

In equation 2.7, the $\sim COH$ groups formed can be looked at as an active intermediate and this can lead to degenerated branching forming functional group structures on the chain:

$$\sim COH(aldehyde) + O_2 \rightarrow \sim \dot{C}O(ketone) + H\dot{O}_2 \quad (2.11)$$

$$\sim \dot{C}O + O_2 \rightarrow \sim CO - O - \dot{O} \quad (2.12)$$

$$\sim CO - O - \dot{O} + \sim CH_2 \sim \rightarrow \sim CO - OOH(peroxy\ acid) + \sim \dot{C}H \sim \quad (2.13)$$

$$\sim CO - O - OH \rightarrow h \sim CO - \dot{O} \sim + hH\dot{O} + (1-h)(products + H_2O) \quad (2.14)$$

$$\sim CO - \dot{O} \rightarrow \sim COOH(carboxylic\ acid) + \sim \dot{C}H \sim + CO_2 + \sim \dot{C}H_2 \quad (2.15)$$

The letters *f, g,* and *h* in equations 2.6,2.10, and 2.14 are the radical efficiency factors which represent how efficient the radicals formed lead to the products [42]. This is needed because the radicals formed could go to other side reactions or to form intermediates than may or may not end up in the products.

2.3 Permeability Theory

To better understand how moisture propagates from the outside of the cable to the inner insulation material, it is necessary to understand permeability of gas or vapor across a polymer membrane. The permeability of a gaseous or liquid component, the permeant, is a measure of its ability to move through the material that resists its passage from one side to another [39]. Concerning this thesis work, the permeant will be water vapor, transmitted across PE film.

When talking about transmission of the permeant across a material, both permeability and permeance are presented together. Although, both terms are connected by the flux of vapor across the film, permeability is what will be calculated in the end for a constant thickness polymer material. The permeability of water vapor is determined gravimetrically using the well-established ASTM method D1653−13 and commercially-available permeation cups from *Gardner Co*. The rate of weight loss ($\dot{m}$, g/hr) is measured by weighing the cups at different time intervals. The calculations leading to the permeability follow the ASTM procedure.

The flux of water across a film is described as the water-vapor transmission rate, WVT, is defined as:

$$WVT = \frac{\dot{m}}{A}, \quad (2.16)$$

where A is the exposed area of the sample. This leads to the definition water-vapor permeance:

$$WVP = \frac{WVT}{\Delta p_{vap}} \tag{2.17}$$

and Δp_{vap} is the difference in the water vapor pressures across the thin film. This value is calculated from the relative humidity on both sides of the film, where it is assumed that saturated conditions exist inside the film. The vapor pressure on both side can be written as:

$$\Delta p_{vap} = p_{sat} - p \tag{2.18}$$

There are many equations that are used to calculate p_{sat}. The one that will be used is the Tetens equation named after the German meteorologist O. Tetens[40]:

$$p_{sat} = 610.78 \times e^{\frac{17.2694*T}{T+238.3}}, \tag{2.19}$$

where T is the temperature in degree Celsius and units of pressure are Pascals. The partial pressure of water vapor on the outside of the film, is calculated from the relative humidity, RH.

$$RH = \frac{p}{p_{sat}}, \tag{2.20}$$

The permeability of the film with thickness L is then:

$$P = L \times WVP = \frac{L \times \dot{m}}{\Delta p_{vap} \times A} \tag{2.21}$$

Typically, the water mass-loss rate is replaced by the volume of water vapor $\dot{V}$ under standard conditions, STP, using the Ideal Gas Law:

$$\dot{V} = \frac{\dot{m}}{M_w} \times \frac{RT^0}{P^0} \tag{2.22}$$

where T^0 and P^0 are the standard temperature (273.15 K) and pressure (one atmosphere), respectively; M_w is the molar mass of water and R is the ideal gas constant (8.314 J/mol K).

The final equation for the calculation of the permeability is:

$$P = \frac{L}{A \times \Delta p_{vap}} \times \frac{\dot{m}}{M_w} \times \frac{RT^0}{P^0} \tag{2.23}$$

For this analysis, some assumptions need to be made for the permeation of water vapor in PE. The PE films used are thin and the polymer backbone is all hydrocarbon chains leading to its nonpolar nature, which are assumed to have no gradient of water vapor within the sample. Therefore, the pressure difference on either side of the film is sufficient which increases linearly. Also, if the water vapor does not interact chemically with the polymer film, the permeability can be expressed as a linear function with the difference in %RH on both sides of the sample. This means that two tests with a varied experimental conditions in terms of difference in %RH for those samples will therefore be enough to tell about the flux for all %RH differences. There are a lot of units that are used to measure of the amount of water vapor penetrated over a fixed area of the material in a given time period. The units used for P, are the Barrer, named after New Zealand chemist Richard Barrer:

$$1 \text{ Barrer} = 10^{-10} \frac{\text{cm} \times (\text{cm}^3_{STP} \text{s}^{-1})}{\text{cm}^2 \times \text{cmHg}}$$

The permeability is often temperature dependent and can be given as an Arrhenius equation as:

$$P = P_0 \times e^{\frac{-E_a}{RT}}, \tag{2.24}$$

where P_0 is the permeation preexponential factor, T is temperature, and E_a is the activation energy of diffusion.

2.4 Diffusion Theory

Diffusion is the movement of molecules solely as a result of a composition difference, which in this case arises from the water concentration within the polymer film on both of the exposed sides. The diffusion coefficient in terms of concentration will be introduced for the one-dimensional case (1-D). This is called Fickian diffusion and it works for most semi-crystalline materials with the appropriate geometry.

The polymer membrane separates the water vapor inside the cup and that outside in the oven environment. From considerations of material transport and the conservation of species, water here, the general 1-D unsteady treatment leads to:

$$\frac{\partial c}{\partial t} = -\frac{\partial}{\partial x} \times J_x, \tag{2.25}$$

where c is the concentration of the diffusing species (i.e. water) within the membrane, t is the time, and J_x is the flux of water in the x direction which is taken as the direction along the thickness of the membrane. For the 1-D treatment to be valid, the area of the membrane surface must be much larger than the thickness (L), specifically A >> L^2, and usually this is satisfied for polymer membranes. Figure 2.3 shows a sketch of the setup of the water, the outside oven environment, and the film clamped over the permeation cup containing the liquid water.

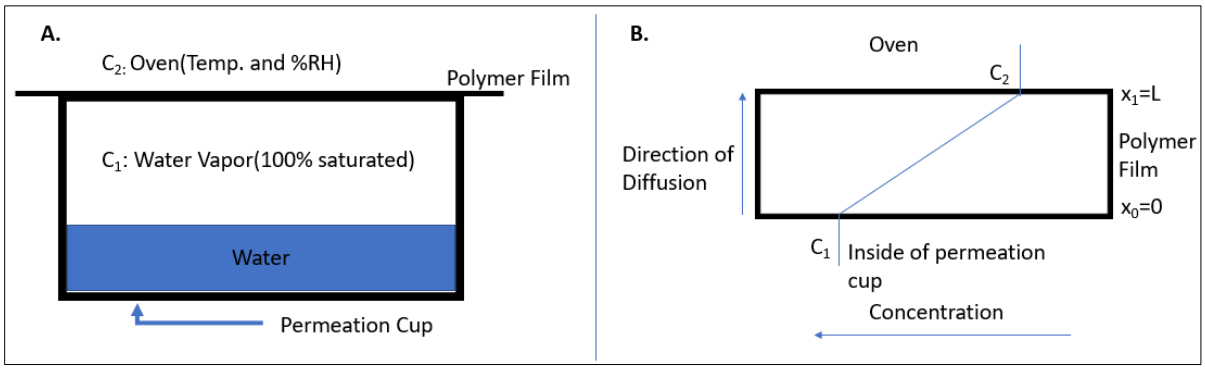

Fig 2.3: On left, A shows the general configuration of the permeation cup and water for modeling purposes. B shows the specific boundaries of importance and the directions of the diffusion and concentration within the film at the polymer membrane-vapor interface for steady-state conditions.

The flux of water, J_x, in the x direction is given by Fick's First Law:

$$J_x = -D \times \frac{\partial c}{\partial x}, \tag{2.26}$$

where D is the diffusion coefficient, which is the proportionality constant that links the molar flux due to the concentration gradient of water. Based on equation 2.26, the diffusion coefficient is assumed to not be dependent on the concentration of the diffusant. But, polymers are often plasticized by solvents such as water resulting in diffusion coefficient being concentration dependent.

To obtain a differential equation connecting the varying concentration with time and the concentration gradient along the thickness, equation 2.26 can be substituted into equation 2.25 to derive Fick's Second Law for a constant diffusion coefficient:

$$\frac{\partial c}{\partial t} = D \times \frac{\partial^2 c}{\partial x^2}, \tag{2.27}$$

Taking the assumptions of steady-state diffusion of water and constant diffusion coefficient, equation 2.27 reduces to:

$$\frac{\partial^2 c}{\partial x^2} = 0, \tag{2.28}$$

Integrating equation 2.28 twice with respect to *x* and introducing boundary conditions at $x = 0$ and L shown in Fig. 2.3, the following solution is obtained:

$$\frac{x}{L} = \frac{c - c_1}{c_2 - c_1}; \tag{2.29}$$

Plugging this solution into equation 2.26 results in:

$$J_x = -D \times \frac{c_2 - c_1}{L} = D \times \frac{c_1 - c_2}{L}, \tag{2.30}$$

To make the connection of the permeability, the flux is the same as the water transmission rate in eq. 2.16:

$$J_x = \frac{\dot{m}}{A} \equiv WVT, \tag{2.31}$$

Using eq. 2.21:

$$P = \frac{L}{\Delta p_{vap}} J_x \; or \; J_x = P \times \frac{\Delta p_{vap}}{L} \tag{2.32}$$

Comparing this to eq. 2.30, the concentrations are within the solid film, whereas the change in water vapor pressure refers to conditions within the vapor phase. These are connected by the solubility, S:

$$c = S \times p \tag{2.33}$$

Equation 2.30 can now be written:

$$J_x = D \times S \times \frac{p_1 - p_2}{L} = D \times S \times \frac{\Delta p_{vap}}{L} \tag{2.34}$$

as $p_1 \equiv p_{sat}$ and $p_2 \equiv p$, shown in eq. 2.18. The comparison with eq. 2.32 shows that:

$$P = D \times S \tag{2.35}$$

So therefore, if the solubility for the diffusing species is known and one of the other coefficients can be determined experimentally, the permeation or diffusion coefficient is calculated from equation 2.35.

It is important to note the term “solubility” here has a meaning distinct from the more common usage as a measure of the composition of a solute in a single phase under well-defined conditions. This solubility relates the composition of one phase to the

composition of another phase at their mutual interface, so it is really a distribution coefficient such as the Henry's constant. An example calculation is given in Appendix B that illustrates this.

CHAPTER 3

3.1 Description of Thesis

With the multitude of studies done on the effects of temperature and radiation on physical, chemical, and electrical properties of XLPE and EPR, there are still some gaps that need to be addressed to better understand accelerated aging for medium and low voltage electrical cables. It is also possible for chemical changes like oxidation to cause degradation of the electrical cable insulation given the right environment. Therefore, there is a need to understand the effects of oxidation and environmental factors that impact the rate of oxidation on polymeric insulation material.

To model the cable aging due to oxidation, aging experiments will have to be developed to model the environments seen in the operating NPPs. By developing such experiments, the oxygen consumption and functionality results can be helpful in determining how this degradation mechanism effects the polymeric insulation material over time. It is important to use and develop the right materials and environment in the research lab to mimic the environment experienced in the NPP at an accelerated rate. Since radiation has been already studied, temperature and pressure of oxygen will be evaluated in terms of water barrier properties.

The primary objective of this thesis is to bridge the temperature and oxygen pressure effects individually and/or as a synergistic effect to see how that effects the physical, chemical, and electrical properties of the polymeric material. To fully model the XLPE and EPR that are used in electrical cable, neat polymer samples of polyethylene (PE) and polypropylene (PP) respectively, will be used but the studies for this thesis will focus on PE. Neat PE samples will be oxidized along with temperature in a closed vessel where oxidation will be modeled by pumping high pressure oxygen gas into the vessel. The timeline for the aging in the vessel will be developed during the thesis. It is possible to have some significant effect on the aging at temperatures from 25°C-80°C. This range is selected because in a combined environment, the inverse effect is postulated to occur, which means that combined environments can cause the polymeric material to degrade more dramatically at lower temperatures as opposed to higher temperatures because cycling and synergistic effects supposedly cause more degradation than a single environmental effect alone . Because of observed temperature effects, an important

aspect of this thesis is the aging needs to be controlled which means the temperature and oxygen pressure need to be well controlled, throughout the aging duration. Another aspect that leads to degradation of cables is immersion where the moisture present in the environment leads degradation and immersion to dielectric breakdown. By taking the most degradative temperature and oxygen pressure and subjecting it to water immersion and moisture environment, a comparison can be made to see what the water adds in terms of the degradation mechanism.

To test the presence of oxidation on the polymer samples is to do chemical characterization using attenuated total reflectance fourier-transform infrared spectroscopy (ATR-FTIR). ATR-FTIR will be used to assess the functional bands in the oxidized polymer material. This will help identify the possible functional groups present in the spectra. Another parameter that will test the performance of the oxidized polymer samples is water vapor permeation which is defined as the water vapor flow through a defined area region which is caused by a pressure difference between the vapor sink and vapor source. The oxidized polymer samples are thought to increase the water vapor flow across the sample.

To evaluate the mechanical properties effects from thermal oxidation, polymer dogbones will be thermally oxidized at the most impactful synergistic temperature/pressure combination. Dogbones will be made using injection molding from pellets and industrial sheet material, differing in molecular weight distribution of polyethylene and processing of the dogbones, used to compare their effects under thermal oxidation. To look at the effects of the oxidation, the stress versus strain and % elongation at break will be plotted in order to see whether the oxidized dogbones are stiffer than the unaged dogbones. Also, any degradation in bulk strength or modulus will be observed quantitatively.

3.2 Literature Search

3.2.1 Accelerated Aging Studies

Before looking at accelerated aging studies, gas flow and sorption behavior was investigated for PE. There are a plethora of papers on this but two papers from the Journal of Polymer Science have studied it rigorously theoretically and experimentally. Looking at flow of gasses first, Alan S. Michaels *et al.,* calculated permeability and diffusion coefficient for amorphous and semi crystalline polymers and calculated permeation, diffusion, and activation energies for each kinetic phenomenon. The four films investigated were made from molding, so the thicknesses varied by 0.024-0.178 cm. The gasses were He, O_2, CO_2, CO, N_2, and many others. What was found was that decreasing the amorphous phase (i.e., increasing the crystallinity) leads to decrease in the permeation and diffusion coefficients [32]. Alan S. Michaels *et al.* also look at sorption and concludes that permeation does not give information on the mechanism but is good for barrier properties. A significant result was shown that the polyethylene is composed of amorphous and crystalline regions where small gas molecules pass through the amorphous regions a lot easier than through the crystalline regions. Thus, it can be considered that amorphous regions of PE act like a porous medium[33].

There have been extensive studies that have assessed the cable insulation in Nuclear Power Plants in all the various chemical, mechanical, and electrical properties [1-3,9−12]. More papers that discuss the properties and aging correlation are mentioned thoroughly in the introduction of this thesis. These studied physical cable insulation taken from NPPs, which are the XLPE and EPR that comprise most insulation. These papers studied the temperature and radiation effect on the aging of the samples. The accelerated aging procedures that were done were temperature alone, radiation alone, temperature/radiation (in that order), and radiation/temperature (in that order) environments. The latter two environments were done sequentially. These accelerated aging resulted in oxidation and free-radical formation, which correlated well with the elongation at break test. Synergism was also discussed, and it depended a lot on the dosage of temperature and radiation. For thermally stable polymers materials like EPR radiation was the dominant effect [1].

Another important aspect related to inverse temperature effects in determining the activation energy for oxidation. We want to be able to age the materials without changing the kinetic mechanism for ageing. By staying in the 20-70°C range, the activation energy can be obtained from the Arrhenius equation. For temperatures greater than 100°C the activation energy was determined to be E_a = 130 kcal/mol and E_a = 63 kcal/mol below 100°C for a tubular EPR specimen(diameter=5mm, thickness=0.8mm) [8]. Similar values have been obtained by other papers for EPR and XLPE [12,18,19]. In these papers, samples were aged in an oven with some samples subjected to various radiation doses.

In this thesis, the main method for determining the effects of oxidation on polyethylene is determining the permeability and diffusion coefficient of water vapor across the film secured in a cup. Values for the permeability of common polymers in different types of gasses was done at 25-30°C [20]. Polyethylene has permeability of 68 Barrer[20]. Because of polyethylene's semi-crystalline nature, the effect of crystalline % on permeability was investigated [20]. Oxygen gas permeability was looked for biaxially oriented molded polypropylene sheets and the calculated value was in between 1−1.12 Barrer depending on the heat treatment of the polypropylene sheets [21]. This was confirmed by other works and other various polymers and elastomers were done as well[22-25]. A. W. Myers *et al.,* studied gas and vapor permeabilities of films and reported permeabilities of different density polyethylene polymers at 25°C [45]. The densities ranged from 0.922 to 0.960 g/cm^3, which corresponded to permeabilities of 900 Barrer and 120 Barrer respectively [45]. The least dense polyethylene, stated in the paper, of 0.922 g/cm^3 gives the permeation activation energy of 33.5 kJ/mol. Diffusion coefficients are just as prominent as permeability and have been studied as well. Alan Michaels and Harris Bixler have calculated values of diffusion for molded polyethylene films with various degrees of the amorphous phase present. Diffusion coefficients, calculated at 25°C for methane, were determined to be 8.9 x 10^{-7} cm^2/s for natural rubber with amorphous fraction of 1.0, and 0.57 x 10^{-7} cm^2/s for polyethylene rubber with amorphous fraction of 0.23 [32]. It was found that with increasing fraction of crystalline phase (i.e. decrease in amorphous phase) resulted in the decrease in diffusion coefficient. David W. McCall *et al.* have found that for the LDPE polymer, diffusion coefficients, done at 25°C, ranged from 10 x 10^{-7} cm^2/s to 0.5 x 10^{-7} cm^2/s with increasing

concentration of oxygen attached to polymer and with increasing solubility of water(ppm) in the polymer, the diffusion coefficients ranged from 8 x 10^{-7} cm^2/s to 4 x 10^{-8} cm^2/s [60]. Table 3.1 summarizes the literature values.

Table 3.1: Summary of the literature values of permeability, diffusion and activation energy with different polymers where some have associated amorphous fraction (α).

Polymer	Density (g/cm^3)	Permeability (Barrer)	Diffusion Coefficient ($cm^2/2$) (x 10^{-7})	Activation Energy (kJ/mol)
Polyethylene	0.922	900	-	33.5
Polyethylene	0.960	120	-	-
Natural rubber (α=1.0)	-	-	8.9 @ 25°C for methane	-
Polyethylene rubber (α=0.23)	-	-	0.57@ 25°C for methane	-
LDPE	-	-	0.5-10 @ 25°C with O_2 & 8-40 with solubility in H_2O	-

With the main goal being to determine the effects of thermal oxidation of polymer films it is logical to review literature. Chabira *et al.*, studied oxidation and crosslinking of LDPE films during thermal aging. They aged neat grade LDPE exempt of stabilizing agents that was melted and then blown into a film. Aging conditions were 70°C in air ventilated oven for as long as 21 months and saw decrease in mechanical properties and decrease in ductility [26]. There was a carbonyl band at 1712 cm^{-1}. Reddy *et al.* examined abiotic and bio-degradation of PE, with an emphasis on abiotic thermal-degradation. PE films were cut and put into loosely screwed glass vials and aged for 2 weeks in 50-70°C in an oven[27]. A carbonyl band was observed at 1735 cm^{-1}, which

increased with increasing aging time. An extensive study on thermal degradation of polyethylene, numerous papers have been cited doing thermal degradation at 80°C and from a range of 150-250°C in an oven [28]. It was noted that the degradation mechanism at higher temperature differs from longer time aging at moderate temperatures [28]. It was found that at 50°C in an oven for 100 days, the carbonyl increased and then stabilized as aging time increased [28]. The papers mentioned so far have been aged in an oven in air. It was difficult to find any mention of the use of a vessel closed-system to do the aging of polymer films. A paper, by Christopher F. Coote *et al.*, done at Worcester Polytechnic Institute in Massachusetts, studied oxidization of ultra-high molecular weight PE (UHMWPE) sheets, which was a good material choice for prosthetic devices [29]. They did accelerated aging tests using Parr Series 4520 bench-top reactor, which is the same manufacturer but different model as used in this thesis. The experiment was done at 70°C in a dry environment with no molecular oxygen gas added inside the reactor for 2 weeks [29]. It was shown that with the accelerated aging, the carbonyl index increased with aging time and moisture did not have a significant effect on the development of the carbonyls. In another experiment, water was added at the bottom of the reactor to simulate humidity and moisture effects. Another potential application of this study can be placed in understanding the permeability behavior of films in barrier materials in food packaging. Valentina Siracusa from University of Catania in Italy studied this for a wide range of polymer films from polyolefins (grades of PE, PP) to substituted olefins (PS) and polyesters (PET) and for a wide range of gasses (N_2, O_2, H_2,CH_4, and many others) [31]. From this study, they determined water vapor and oxygen gas are important permeants for looking at shelf-life and product quality because of their ability to move through the polymer film wall from internally or externally. Also, they found that when oxygen was the permeant for HDPE, the permeability decreased as the crystallinity increased. Outside of thermal oxidation studies, work by Ibukun Oluwoye *et al.* explored theoretical modeling of lower temperature oxidation, meaning below the softening point, of polyethylene films in NO_x (x=1 or 2) environments. The motivation was because NO_x gasses, at slightly elevated temperatures, are much more aggressive and toxic than O_2 gas. By assuming an orthorhombic PE unit cell and the NO_x molecule reacting at the target region of the PE chains. The possible reaction pathways for PE in a NO_x

atmosphere was sketched [30]. The mechanism for initiation step and formation of oxides, nitrates, and nitrites products was determined. The thermodynamics and kinetic parameters were calculated for the radical reactions and their intermediates [30]. This study mentions that this can help provide insight of the effects of industrial pollutants on polymers.

As for immersion effects of water in oxygen rich environment, the solubilities of oxygen gas in water needs to be considered. There is a large database of studies that have done so for a wide range of temperatures from 273 to ~ 617K. Majority of the papers had done studies at oxygen pressures of 1 bar. Fox *et al.,* determined the volume of O_2 gas taken up and volume absorbed which increased and decreased respectively up to 50°C[46]. Shchukarev *et al.,* determined that water behavior towards gasses of low solubility such as oxygen is rather peculiar [47]. With increasing temperature, their solubility decreases at first, passes through an absolute minimum depending on the gas, and then increases [47]. The minimum solubility occurs between 60°C and 90°C and is 80°C for oxygen gas specifically. Solubility was determined using the Ostwald coefficient relating the volume of gas dissolved in one volume of solvent(liquid) and for 50°C it was 0.0238. Wise *et al.,* had also determined solubility values from 10°C to 60°C and for 60°C the solubility value was 19.5 mL/1000g [48]. The same decrease in solubility was seen with increasing temperature. Few papers have done studies very high oxygen pressures as high as 100 and 200 bar [49,50]. Interestingly, Pray *et al.*, experimented oxygen pressures from 6.89 to 27.6 bar [51]. It was found that, at temperatures from 435.5 to 616.5 K, the solubility (mL O_2/g H_2O) increased linearly up to 616.5K with increasing partial pressure up to 700 psia. The solubility with respect to temperature showed a parabolic nature where the minimum is ~125℃ at these higher pressures [51]. For water solubility in water for branched polyethylene, the range is 15-20 ppm [60].

Many studies have been explored the role of temperature and radiation effects on mechanical properties such as elongation and tensile strength. A study by Balasubramanian Suresh *et al.,* used pristine blown film LDPE films, along with oxo-biodegradable additive, subjected to thermal aging at 70°C in an oven for various treatment times and found that the elongation at break and tensile strength decreased with

increasing treatment time [52]. Similar experiments have been done with synergistic temperature/radiation aging over various times but at higher temperatures. Oven aging of EPR and XLPE was also done at 155 and 175°C and also with Co-60 gamma radiation of 10kGy/hr [8]. K.T. Gillen *et al.* used four EPR insulation cables from different manufacturers which have retardants in them. Accelerated aging was done on strips of the material in the oven from 101 to 170°C and temperatures in between. It was found that the elongation at break decreased more dramatically at higher temperature which took less time to degrade the EPR [53]. Hyun Jeong Jeon *et al.* investigated, using Iron 3+ stearate complex additive, Linear Low-Density Polyethylene (LLDPE) film in order to biodegrade it. It was found that increasing the temperature at the same UV exposure duration of 70 hours from 30 to 50°C decreased % strain at the maximum (Ultimate Tensile Strength) and at the yield point. Also, if the intensity of UV exposure and temperature(40°C) is constant, it was found that increasing the exposure time decreased the % strain at the maximum and at the yield point [54]. A different study was done on accelerated aging of polypropylene (PP) injected with antioxidants to look at its degradation in chlorine water, deionized water and air for 30−120 days at temperatures of 23, 60, and 80°C. It was found that the tensile strength initially increased and then decreased as treatment time increased contrary to PE [55]. This trend was the case for all the temperatures and mediums [55]. J. Wise *et al.*, determined the modulus profiles, which has recently been developed to look at oxidation of polymers, of 0.2cm and 0.22cm thick nitrile rubber and 2-chlorobuta−1,3-diene (Neoprene) respectively [56]. The modulus profile is similar to the commonly measured tensile modulus. It was found that, for a range from 65 to 150°C for both rubbers, the modulus (MPa) was a convex parabolic profile and with increasing depth exposure to the surface up to 50% depth [56]. The extent of convexity increases with oxidation time and temperature [56].

CHAPTER 4

4.1 Materials

Fifty-micron thick LDPE pristine films, (Goodfellow Cambridge Limited) were used for this study. The molecular weight distribution provided from supplier is around 400,000 g/mol. The pristine films were cut into 10.16 by 10.16cm (uncertainty of ± 1.27cm) squares, which had an average mass of 0.48± 0.06 g for the 50 µm films for the experiments to follow.

4.2 Thermal Oxidation Simulation

The LDPE films were exposed to oxygen in 2-L pressure vessel (Parr Instruments, 4600 series) and its temperature was controlled (Parr Instruments, 4838 PID controller) under proportional-only control to avoid overshooting the desired temperature, upon startup. The surrounding laboratory ambient temperature was around 22-23°C. The films were placed in the vessel and spread out so that there no films were stuck together, and the surfaces were accessible by the oxygen gas. Oxygen gas from a compressed gas tank was transferred into the vessel to induce the oxygen-rich environment and then the temperature was raised. Experiments were done at 30 and 50psi oxygen pressures (oxygen pressure prior to raising the temperature) and four temperatures (22, 50, 70, and 80°C). WinDaq data acquisition software was used to monitor the temperature profile on the outside and inside of the vessel. The oxidation durations were done for 19 and 33 days. Figure 4.1A shows the setup used when used during the experiment.

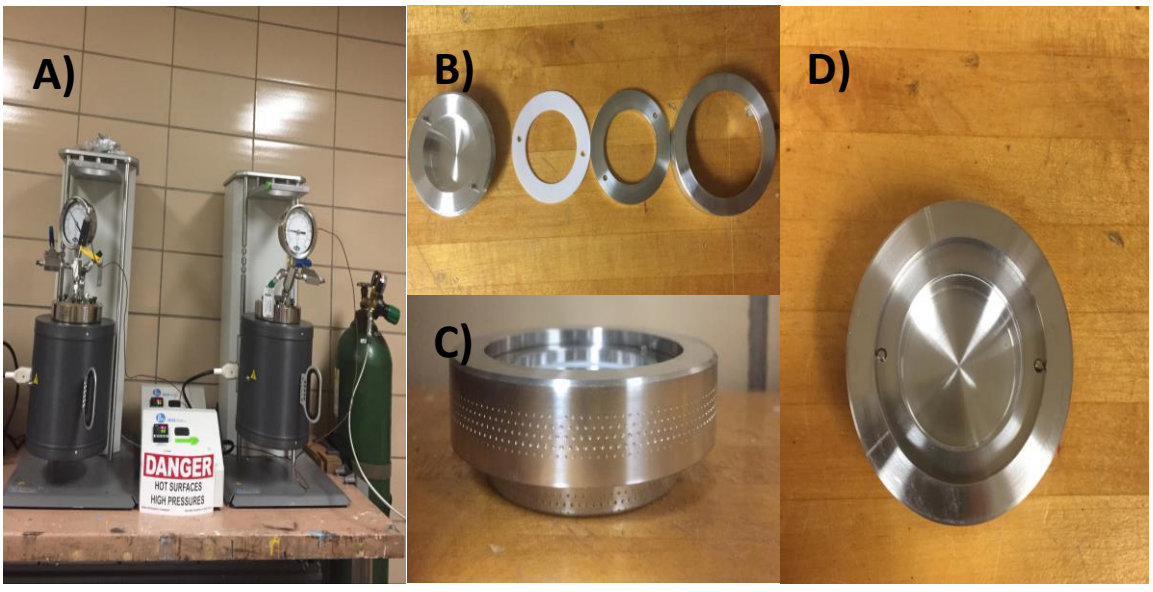

Fig 4.1: A) Experimental setup of the Parr Instrument vessels next to each other used. On the right most, side is the oxygen tank used to supply the oxygen gas. B) Parts of the permeation cup when it is ready to be assembled for LDPE permeation test going from left to right. The film is put on first and then the PTFE white gasket. Figs C and D show a fully assembled permeation not including the film.

4.2.1 Thermal Oxidation with Immersion

To initially investigate the effects of oxygen pressure in combination with water, the most oxidative condition, 80°C and 50 psi, was used. The Parr vessel was filled with 1-L of D.I. water in which ten 50μm LDPE films were immersed in water. The films were cut into 10.16 by 10.16cm (uncertainty of ± 1.27cm) squares with average mass of 0.46 ± 0.02 g. Films of the same size and with an average mass of 0.43 ± 0.02 g were kept above the water inside the Parr vessel for comparison. The oxidation durations were done for 19 and 33 days. At each duration, a sample of the water was taken for pH analysis (instrument accuracy ±0.002 pH) and the films were dried with Kim wipes and weighed to record changes in mass. Because of the placement of the films in the Parr vessel, the films above the water will be called Wet-Gaseous Oxygen (WGO) films and the films submerged in the water will be called Aqueous Dissolved Oxygen (AGO) films. The films that were done as described in previous section will be called Dry O_2 because only the films and oxygen gas were present in the vessel.

4.2.2 Mechanical Properties Investigation

ACME plastic sheet material Protec PP (density 0.9 g/cm^3 & 151°C softening point) and Hitec HDPE (density 0.96 g/cm^3 & 129°C softening point) was used to cut out Type IV from ASTM D638−14 standard dogbones to investigate the degradation in mechanical properties. They then were subjected to 70°C and 30psi oxygen pressure (prior to raising the temperature) in the 2-L Parr vessel for oxidation durations of 2 months. The dogbones were separated so that the gauge-lengths were not touching each other. Dogbones were also made by injection molding LDPE, High-Density Polyethylene (HDPE), and High-Density Polypropylene (HDPP) from Sigma Aldrich onto Type IV dogbone shape. Table 4.1 shows the relevant properties for each polymer material. A total of 48 dogbones were made in which 12 of each polymer materials were made along with four of each for control samples. The dogbones were subjected to the same 70°C

and 30psi oxygen pressure in the Parr vessel for 3 months in which four of each type was taken out every 1 month to test mechanical properties which are Elastic Modulus, Ultimate Tensile Strength (UTS), and strain at UTS or elongation. The instrument used was the MTS Landmark Servo-Hydraulic Test System. The temperature and relative humidity of the laboratory was 21.4±0.3°C and 10.0±0.3%. The load rate using 2kN lower load cell and 250kN upper load cell was 5 mm/min.

Table 4.1: Properties and relevant information about the polymers used for mechanical testing effects from thermal oxidation.

Polymer	Melt Index (g/10 min)	Melt Point (°C)	Avg. M_w (g/mol, by GPC)	Avg. M_n (g/mol, by GPC)	Density (g/mL @ 25°C)	Physical Form
LDPE	2250	90	35,000	7,700	0.906	powder
HDPE	12	125−140	72,463	-	0.952	pellet
HDPP (isotactic)	4	160−165	340,000	97,000	0.90	pellet

4.3 Chemical Property Tests

4.3.1 Permeation Cup Test

Oxidized films were cut into circles to fit in the 12cm^2 cross section of the cups (Paul N. Gardner Company Inc.) used for the permeation test. The permeation test was prepared and followed according to the wet cup test in ASTM D1653−13 for 14-day durations to obtain the mass loss vs time for the permeation calculation. In each experiment, it was ensured a pristine 50 μm LDPE film was run alongside the oxidized film. The permeation cups were put in an oven film side using oven temperatures of 60, 70, and 90°C. The ambient laboratory temperature(±1°C) and relative humidity(± 1.5% RH) were monitored outside the oven throughout each experiment. Figures 4.1B to 4.1D show the permeation cups when taken apart and assembled.

4.3.2 Attenuated Total Reflectance-Fourier Transform Infrared Spectroscopy

To determine the extent of oxidation, Attenuated Total Reflectance Fourier-Transform Infrared Spectroscopy (ATR-FTIR), with a Thermoscientific Nicolet iS10

instrument, was used to measure the absorbances of the carbonyl peaks. Pristine film was run alongside the oxidized film. For oxidation, the carbonyl peak from 1700cm^{-1} to 1740cm^{-1} was observed if oxidation occurred. To measure the extent of oxidation over the whole film, three scans on each side were done giving a total of six scans for a single oxidized film. The extent of oxidation was quantified by peak integrations (IGOR Pro 8 software). The carbonyl group peaks were integrated from 1690 to 1780cm^{-1} and those for the methyl group peaks from 1320 to 1400 cm^{-1}. The carbonyl peaks areas were then normalized with respect to the methyl group peaks area, which defines the carbonyl index.

4.3.3 Thermogravimetric Analysis

Thermogravimetric analysis (TGA) was done on the oxidized PE films, comparing it to pristine PE film, to measure the change in weight during the heating process. The TGA instrument used was TA Instruments Discovery 550 with platinum pans. Four hole-punched (6.0±0.5mm diameter with average mass of 7.68±0.39 mg) circles were prepared from the pristine and oxidized films and were stacked up into 4 layers of film. The procedure ran was: N_2 purge, heating rate of 5°C/min up to 500°C, isothermal for 10 mins, O_2 purge, and finally isothermal for 30 minutes. The resulting plots were analyzed using the TA Universal Analysis software. To compare the pristine and the various oxidized PE films, temperature at 10/50/90% weight loss and onset point values were determined.

CHAPTER 5

5.1 Results and Discussion

5.1.1 ATR-FTIR Spectra

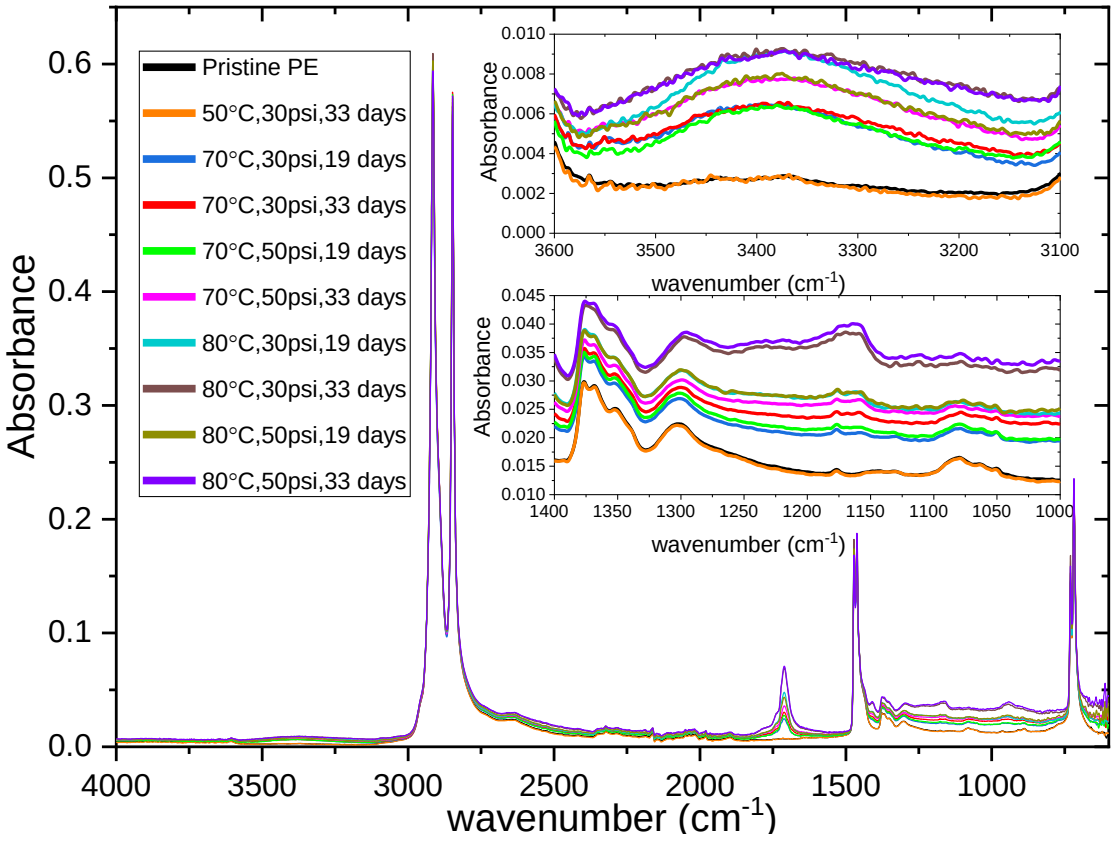

Fig 5.1: FTIR spectra of the LDPE subjected to thermal oxidation in the Parr vessel at four temperatures (room temperature 22, 50, 70, & 80°C) at oxygen pressures of 30psi or 50psi for 19 or 33 days. *Upper Inset:* FTIR spectra from 3100 to 3600 cm^{-1}. *Lower Inset:* FTIR spectra from 1000 to 1400 cm^{-1}.

FTIR spectra are commonly used in determining the functionality of the products formed in the surface of films [57]. Shown in Figure 5.1 and its two inset plots are the spectra of interest. The carbonyl index was calculated from the spectra and it is defined as the concentration of carbonyl products normalized to the methyl C-H bands. In Figure 5.1, there is a sharp band at 1711 cm^{-1} that increases as the temperature, treatment time, and oxygen pressure increases. Bands are present in the region from 3100 to 3600 cm^{-1} and from 1000 to 1400 cm^{-1}. Experimental conditions of 80°C & 50 psi of oxygen pressure, for 33 days yield absorbances close to 0.01 and greater than 0.03 for 3100 to 3600 cm^{-1} and 1000 to 1400 cm^{-1} respectively. The increase in the broad band from 3100 to 3600 cm^{-1}` can be attributed to O-H stretches. At 3373 cm^{-1}, the absorbance takes is at

a maximum. Medium bands are present in the 1000 to 1400 cm^{-1} where bands at ~1155 cm^{-1} and 1362 cm^{-1} belong to ester stretches.

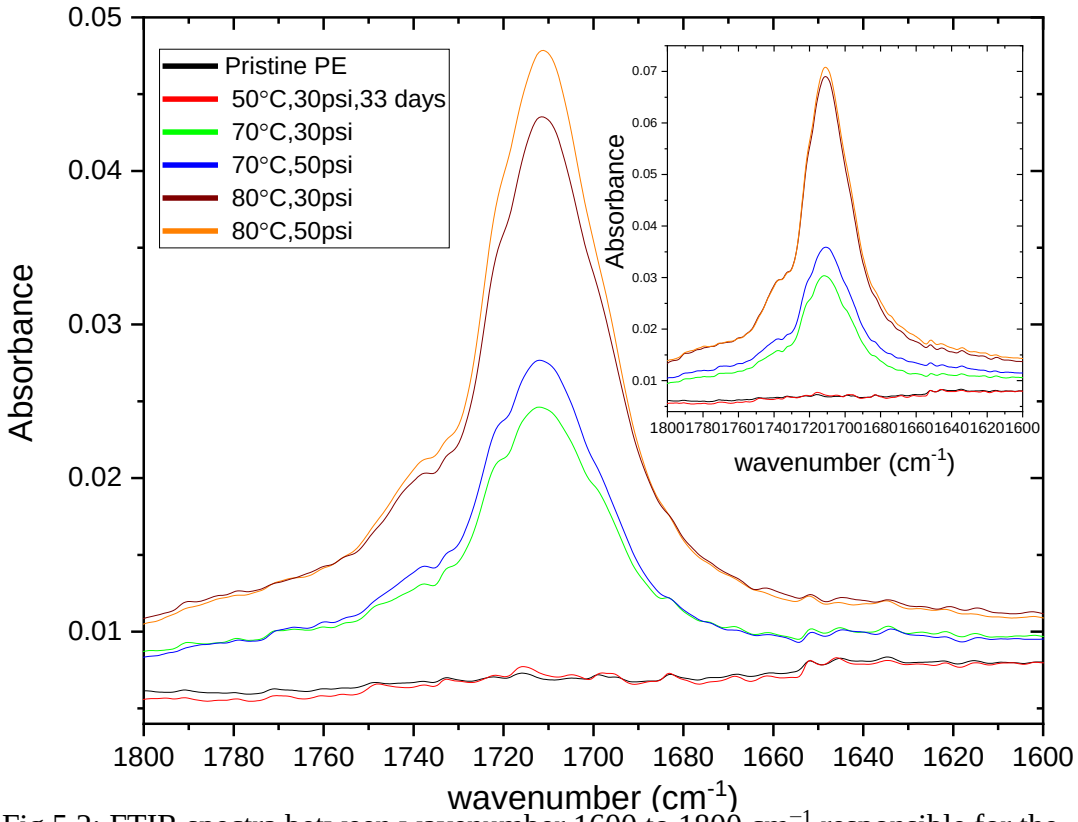

Fig 5.2: FTIR spectra between wavenumber 1600 to 1800 cm^{-1} responsible for the carbonyl functional groups forming on the LDPE film after 19 days of aging. *Upper Inset:* Shows the same 1600 to 1800 cm^{-1} region but for 33 days of aging. The legend applies for both the plot and inset plot.

The strong band at 1711 cm^{-1} shown in Figure 5.2 is the clear indication of carbonyl products present in the LDPE film. This band can be attributed to the ketonic carbonyl and carboxylic acid carbonyl groups formed on the LDPE film as it being oxidized and the band increases with the temperature, treatment time, and oxygen pressure [58-59]. The same 80°C and 50 psi of oxygen pressure lead to largest absorbances which are 0.047 and 0.071 for 19 and 33 days respectively. A hump or shoulder in the band is also present. This shoulder at ~ 1735 cm^{-1} can be attributed to the formation of esters upon oxidation [58]. Another shoulder band at ~1720 cm^{-1}, belongs to the ketone, carboxylic acids, aldehydes, and esters formed via Norrish I reaction mechanism [26]. As the absorbances increase, the ~1720 cm^{-1} band seems to disappear. This is present when aged for 19 and 33 days as seen in Figure 5.2 and the inset plot. We

hypothesize that increased temperature and oxidation time allows for the more of the oxidation products to form, which are the carboxylic acid and ketone groups [59]. This is supported by Iring *et al.* who determined that the kinetics of the aldehyde formation is very fast at high oxygen pressures and this is a secondary process [59]. From this, it can be said that as the oxidation of LDPE progresses, the ketone carbonyl groups become the dominant products are the further oxidized result of the aldehyde group products.

5.2 Permeability and Carbonyl Index

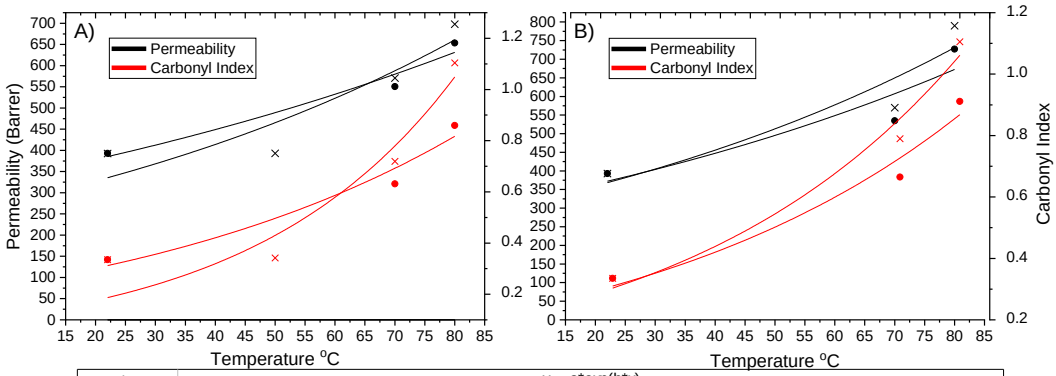

Equation	y = a*exp(b*x)			
Plot	Permeability- 19 days	Permeability- 33 days	Carbonyl Index- 19 days	Carbonyl Index- 33 days
a	319	259	0.216	0.097
b	0.009	0.012	0.017	0.03
R-Squared	0.96	0.847	0.956	0.91

Equation	y = a*exp(b*x)			
Plot	Permeability- 19 days	Permeability- 33 days	Carbonyl Index- 19 days	Carbonyl Index- 33 days
a	297	284	0.21	0.189
b	0.01	0.012	0.018	0.022
R-Squared	0.846	0.868	0.962	0.976

Fig 5.3: Permeability and carbonyl index values as a function of temperature for the LDPE thin films subjected to the thermal oxidation at four temperatures (room temp 22, 50, 70, & 80°C) for 19 (○) and 33 (X) days using 30psi, in *5.3A*, and 50 psi, in *5.3B*, of oxygen pressure. Exponential fit was done in which the upper table refers to fig 5.3A and the lower table refers to fig 5.3B.

The carbonyl index is the way to quantify the concentration of carbonyl functional groups in the film. As shown in figures 5.3A and 5.3B, both permeability of water vapor and carbonyl index (C.I.) are plotted together. The permeability increases steeply from 50 to 80°C and the same occurs with the carbonyl index for both 30 and 50 psi oxygen pressure. An exponential fit was done on the data because of the Arrhenius relationship shown in equation 2.24 between temperature and permeability. Also, an exponential fit indicates that the oxidation reaction order is first order which is a good first level of approximation of understanding the oxidation. At 80°C and 50 psi, of oxygen pressure

and treatment time of 33 days, the permeability and carbonyl index are 790 Barrer and 1.10, respectively. This value of permeability values corresponds well with the 120-900 Barrer range mentioned elsewhere[45]. This can be explained by the fact that polyethylene is modeled as a semi-crystalline polymer with regions of crystalline and amorphous regions. The amorphous regions are made of polymer web-like structures where the holes represent the amorphous regions for which the gas molecules go through [32]. It has been determined that these amorphous regions serve as areas of lower activation energy for the gas molecules to permeate, as in these areas the polymer chains lack crystalline structure and therefore cannot immobilize the gas molecules from moving through the film [17]. It was also thought that the localized charged oxidized regions may act as a barrier for oxygen advancement. Though, this would require more work to better understand the mechanism of gas molecular advancement.

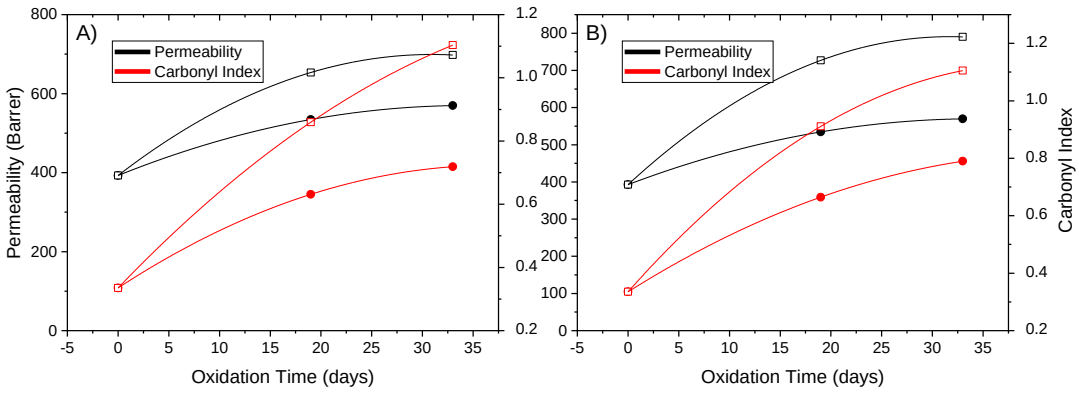

Equation	y = Intercept + B1*x^1 + B2*x^2			
Plot	Permeability- 19 days	Permeability- 19 days	Carbonyl Index- 19 days	Carbonyl Index- 33 days
Weight	No Weighting			
Intercept	393	393	0.335	0.335
B1	10.1	19.8	0.021	0.033
B2	-0.15	-0.32	-2.832E-4	-3.085E-4
R-Squared	1	1	1	1

Equation	y = Intercept + B1*x^1 + B2*x^2			
Plot	Permeability- 19 days	Permeability- 33 days	Carbonyl Index- 19 days	Carbonyl Index- 33 days
Weight	No Weighting			
Intercept	393	393	0.335	0.335
B1	10.1	25.1	0.022	0.04
B2	-0.15	-0.396	-2.552E-4	-4.984E-4
R-Squared	1	1	1	1

Fig 5.4: Shows the permeability and carbonyl index values against oxidation time for LDPE thin films LDPE subjected to thermal oxidation at four temperatures (22, 50, 70, & 80°C) for 19 (○) and 33 (□) days using 30psi, in *5.4A*, and in 50 psi, in *5.4B*, of oxygen pressure. Power law (n=2) was done in which the upper table refers to fig 5.4A and the lower table refers to fig 5.4B.

Figures 5.4A and 5.4B shows quantitively the permeability of water vapor and the carbonyl index as in Figure 5.3 but now with respect to oxidation treatment time. An initial power law was done with the data points available, and more data points in the oxidation times would be needed to justify the trend. Although, three data points is insufficient, it can help to provide as to whether there is a permeability values level off after a certain amount of time of oxidation. As oxidation time increases, both quantities increase, which is the same trend as seen with temperature in Fig. 5.3. The relationship between permeability and carbonyl index looks to be a power law with increasing oxidation time given the number of data points. Also, there is a dramatic increase from pristine unaged LDPE to 19 days, but less of an increase from 19 to 33 days. The same phenomenon is observed when looking at the carbonyl indexes in Figures 5.4A and 5.4B. Looking at Figure 5.4B for 50psi oxygen pressure, the carbonyl index increased 98.3% and 171% from pristine LDPE to 19 days for 70 and 80°C respectively. From 19 to 33 days, it only increased 18.8% and 21.3% for 70 and 80°C, respectively. This can be explained by the fact that low activation energy region must be concentrated enough to have the chain segments lack local order [32]. As temperature and treatment time increase, the chains mobilize so that they relax in a favorable thermodynamic chain structure to allow water vapor to flow through the amorphous region.

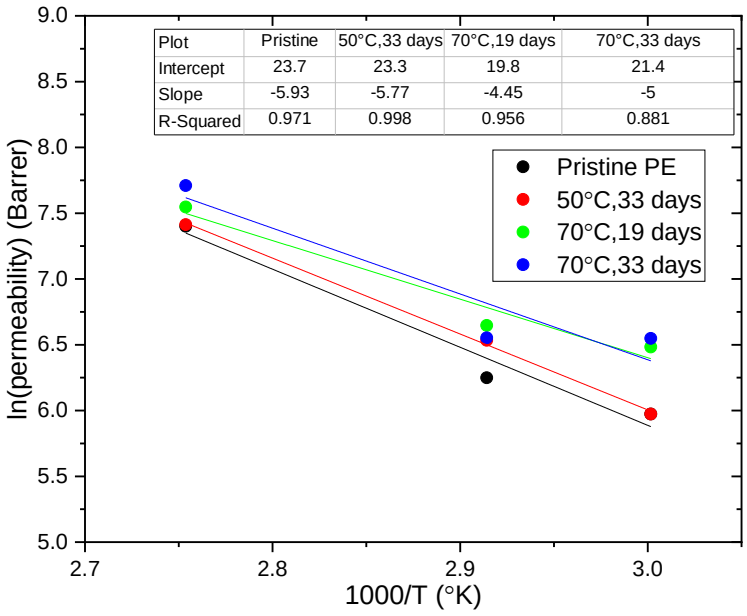

Fig 5.5: Permeability of the aged LDPE thin film done at 60,70, and 90°C for constant 30 psi oxygen pressure as well as linear regression for activation energy calculation.

To determine an activation energy for the flow of water vapor across the oxidized LDPE films the permeability cup test must be done at different temperatures as shown in Figure 5.5. The activation energy would represent the activation energy of the water vapor moving across the film and the influence of temperature[32]. Activation energies, in kJ/mol, are calculated and shown in Table 5.1 by taking the slopes in the table in fig. 5.5 and multiplying by the Ideal Gas Constant of 8.314 J/mol K. As the temperature and treatment oxidation time increase, the activation energy decreases. This behavior has been described for molecules with similar molecular weight as water vapor such as methane and carbon dioxide [32]. Also, the values determined are within 40% from the 33.5 kJ/mol reported for 0.922 g/cm^3 polyethylene from 10 to 90°C [45].

Table 5.1: Shows the activation energies for water vapor transport across LDPE film from Fig. 5.5.

Temp. (°C)	Oxygen pressure (psig)	Oxidation time (days)	Activation Energy (kJ/mol)
22	0	0	49
50	30	33	48
70	30	19	42
70	30	33	37

5.3 Immersed Polyethylene Study

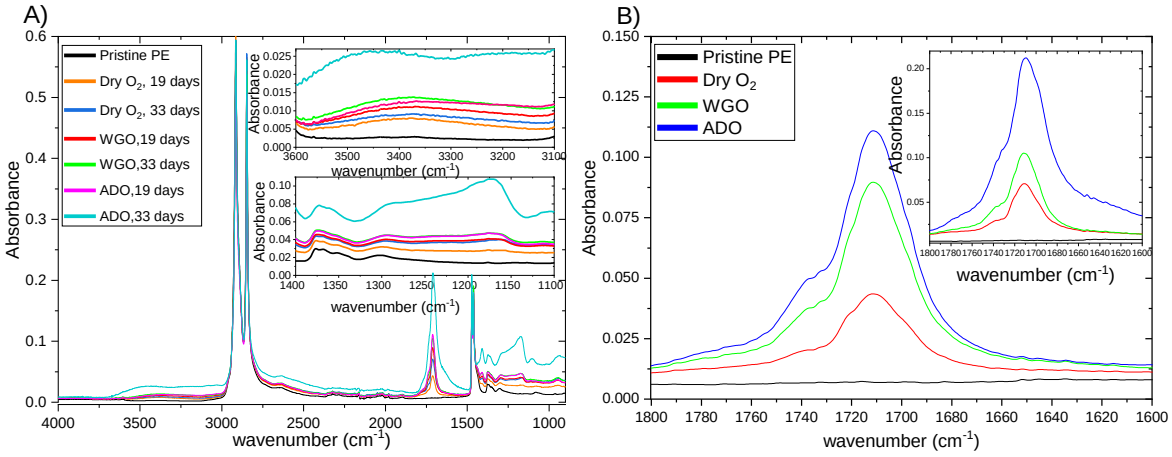

Fig 5.6: A) FTIR spectra of the LDPE subjected to thermal oxidation in the Parr vessel constant 80°C at 50 psi oxygen pressure for 19 and 33 days comparing the Dry O_2 to the WGO and ADO film samples as discussed in the Experiments section. *Upper Inset:* FTIR spectra from 3100 to 3600 cm^{-1}. *Lower Inset:* FTIR spectra from 1000 to 1400 cm^{-1}. B)

FTIR spectra between wavenumber 1600 to 1800 cm^{-1} responsible for the carbonyl functional groups forming on the LDPE film for immersion conditions in Experiment section. The legend applies for both the plot and its inset plot. *Upper Inset:* Shows the same 1600 to 1800 cm^{-1} region but for 33 days of aging.

A similar analysis as in Figure 5.1 and 5.2 can be used to explain the presence of the O-H stretches shown in Figure 5.6A upper inset plot, the ester bands are present in the 1000 to 1400 cm^{-1} in Figure 5.6A lower inset plot and ketonic and carboxylic carbonyl acid groups in Figure 5.6B. The WGO and ADO films had significantly higher absorbances than a dry environment where no water is present, and this trend is consistent with the oxidation time. At elevated temperatures below the melting point, the polyethylene become mobile enough to allow water to move through the amorphous phase regions and pores which contribute to the higher absorbances observed and the overlapping of the bands

In Figure 5.6A upper inset plot, there looks to be overlap at certain wavenumber ranges from 3100 to 3600 cm^{-1} which could be explained by the inconsistencies in the FTIR collection is that some surfaces of the film were not as saturated with water. Alternatively, at a given aging duration, the WGO films were in more of an oxidative environment at long times than the ADO films at shorter times. The ADO films for 33 days yield higher absorbances shown in figs 5.6A and 5.B at all the wavenumber regions. In Figure 5.6A lower plot, there is a noticeable band at ~1170cm^{-1} that was not present with the films subjected to dry O_2 condition, which shows ester C-O formation. Bands in 1350 to 1400 cm^{-1} are possibly due to overlap of esters, aldehydes, and carboxylic acids. Other noticeable bands in the finger print region are at ~933cm^{-1} and ~1104cm^{-1}, which collectively contribute to the stretching and bending of the -CH_2 due to the thermal molecular motions.

In Figure 5.6B, shows clearly the ketone and carboxylic carbonyl groups at ~1711cm^{-1}. The trend of the WGO and ADO films is similar to the dry oxygen gas condition except the absorbances are twice as large for the films above the water and three times as large for the immersed films. This is consistent at 19 and 33 days. As noted in Figure 5.2, there is a shoulder band at ~1720cm^{-1} that disappears at the temperature, oxygen pressure, and oxidation duration increased. The shoulder band is close to nonexistent with the immersed samples which leads to a band that is not broad. This was

explained by Salem f. Chabira *et al.*, by discussing the Norrish I mechanism which carboxylic acids were formed from ketone groups [26]. This would lead to significant weakening of the film and later embrittlement, which was consistent with the ADO film samples seen visually. Another band forms at ~1739cm^{-1} which is responsible for the ester and aldehyde formation.

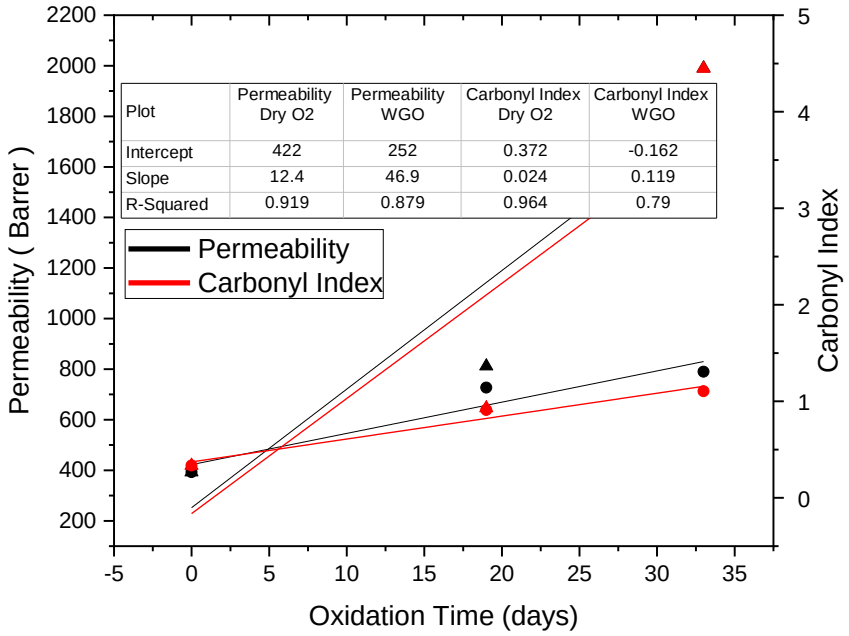

Fig 5.7: Permeability and carbonyl index values of the Dry O_2 (○) and the WGO (▲) against treatment time for LDPE thin films LDPE subjected to constant 80°C and 50 psi oxygen gas in water environment as mentioned in experiment section. The ADO aged film samples lost their integrity and ripped before they could be put into the permeation cup, so permeation cup test could not be done but carbonyl index was determined.

Figure 5.7 compares films in oxygen gas only environment to the WGO films and it can be seen that the WGO films had slightly larger permeability and carbonyl index at 19 days. At longer, times the difference between the two aging conditions became significantly larger at 33 days, where the WGO films had 1990 Barrer and 4.45 for permeability and carbonyl index respectively. The relationship at the higher temperatures range including control samples is linear. The strength of the linearity is better if the control sample data was not included. It can be said that up to 80°C, the relationship shows linear trend as the temperature has not approached a significant temperature were the film microstructure drastically changes. The larger permeabilities can be explained similarly as in Figures 5.3 and 5.4, in that at elevated temperatures the polyethylene

chains become highly mobile, which gives better ability of the water vapor in the cup to permeate through the film. Looking specifically at when the films are in the Parr vessel. At the 80°C and 50 psi oxygen gas with water, there seem to be competing processes in terms of interacting with the film including the oxygen gas and the moisture that adheres along the film. It is difficult to say at this point as to which prevails but the synergism of the two environments helped the degradation to propagate deeper into the film. Similar to the Dry O_2, a possible mechanism is that the elevated temperatures the oxygen is oxidizing the amorphous region of the polyethylene which creates a buffer region to prevent further oxidation which entail acts like a crystalline region [62]. This added on with the crystalline region increases the crystallinity overall taking longer times since now there is an additional barrier of the oxygen gas and water to go through. At these areas of oxidation in the amorphous region, it is possible that the moisture adhered to the film is moving inside the film and there is an additional interaction of the oxidized moieties in the film and the water[60]. Yet, David W. McCall *et al.*, study have suggested that it is indeed the water than moves through the amorphous-only region where oxidation has not come in contact with the film [60]. In a sense the water is finding the path of least resistance.

The ADO films, even though not shown in Figure 5.7, had even larger carbonyl index that was 10.6, a little more than twice of the films above the water. If the films were placed in a way so that the film did not rip when it was tested in the permeation cup, it would be predicted that the permeability would be greater than 1990 Barrer. Since the films are completely immersed in the water, there is no direct interaction of the films with the oxygen gas, but there is oxygen solubility extent in the water that will change the water concentrations. To see chemical changes in the water during the entire experiment, a sample of the water was taken at 19 and 33 days and compared to D.I. water. The pH of D.I., which was 8.318±0.120, water was difficult to determine accurately because of the external environmental influencing the value. The pH at 19 and 33 days of oxidative aging in the Parr was 3.360±0.007 and 3.05±0.03, respectively, indicating a significant acidic environment using 95% confidence ($p<0.05$) using ANOVA. A deeper analysis would be needed to analyze what compounds could be present that leached from the LDPE film into the water contributing to the acidity. In predicting the amount of oxygen

in the water, Ming Geng and Zhenhao Duan have compiled an extensive analysis of oxygen solubility in water with temperature and oxygen pressure dependences, an approximate value can be made based on 1 bar oxygen pressure [61]. At 80°C, the amount of oxygen at 1 bar is 0.008 molal, so therefore at 50 psi(3.45bar) it could be postulated that the amount of oxygen is three to five times more than at 1 bar (0.0024-0.004 molal) [61].

5.4 Kinetic Mechanism of LDPE Thermal Oxidation

To better understand the functional products that can form when the LDPE film was thermally oxidized, it is useful to use the previous FTIR spectra to show what the structure of the possible products that can be formed. Whether the films are exposed to direct oxygen gas(Dry O_2), ADO, and WGO, the spectra indicate carbonyl products present in the LDPE film, which can be attributed to the ketonic carbonyl and carboxylic acid carbonyl groups formed. Secondary functional products are present at low extents of thermal oxidation, which are aldehydes and esters. This was all postulated and structured out by Iring *et al.* [59]. The shoulder bands indicate a contribution of many intermediates that can be formed which was well captured by Oluwoye *et al.* and their computational approach [62].

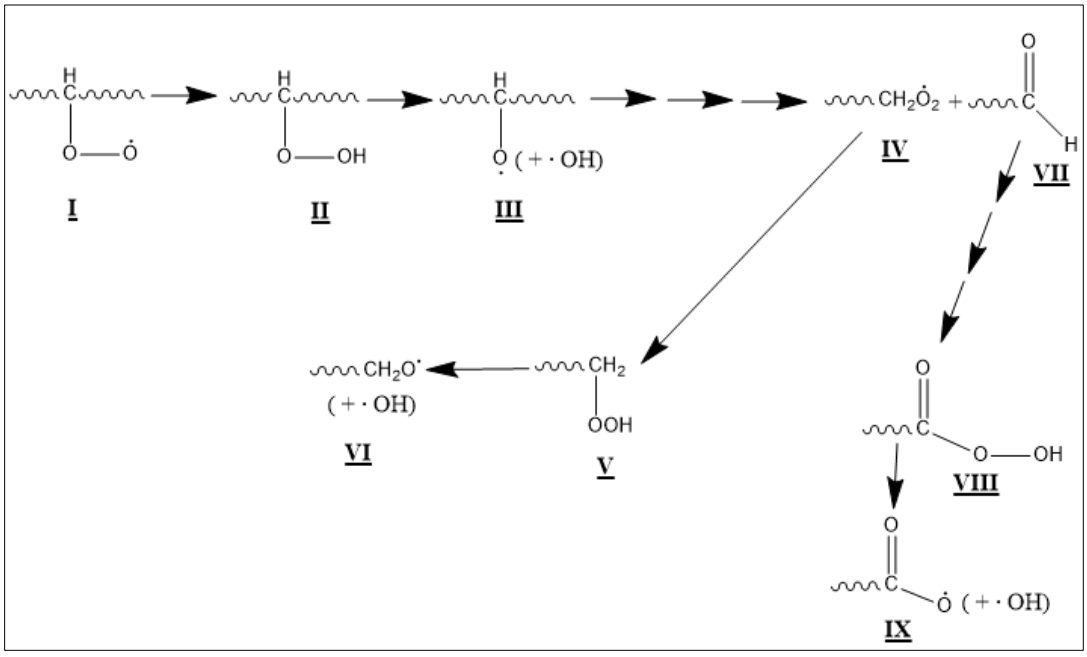

Fig 5.8: Molecular structure of the intermediates of polyethylene oxidation that lead to the products later on[59].

Figure 5.8 shows the possibilities of the functionality groups on the polyethylene chain during the thermal oxidation and degradation and they can be justified to some extent using the FTIR results. From intermediate I, the radical oxidation product is formed that can later be attacked by hydrogen atoms from neighboring chains. Hydroperoxide in II is formed which can be decomposed into a peroxy ROO* in III which leads to carboxylic acid formation on the chain. Aldehydes (in VII) can form which are derived from decomposing the hydroperoxide and then the radical acquires a hydrogen thus forming an aldehyde (~CH=O) as well as more radicals to propagate the oxidation. It can be noticed that practically all of the intermediates have many variations of carbon bonded to oxygen whether it is single or double bonded. This collectively may explain the overlap in the bands in the fingerprint region and in the carbonyl band. The aldehyde can be further reacted with oxygen and other radicals present to form ketone radicals, carboxylate RCOO* radicals, and peroxy RCOOO* radicals.

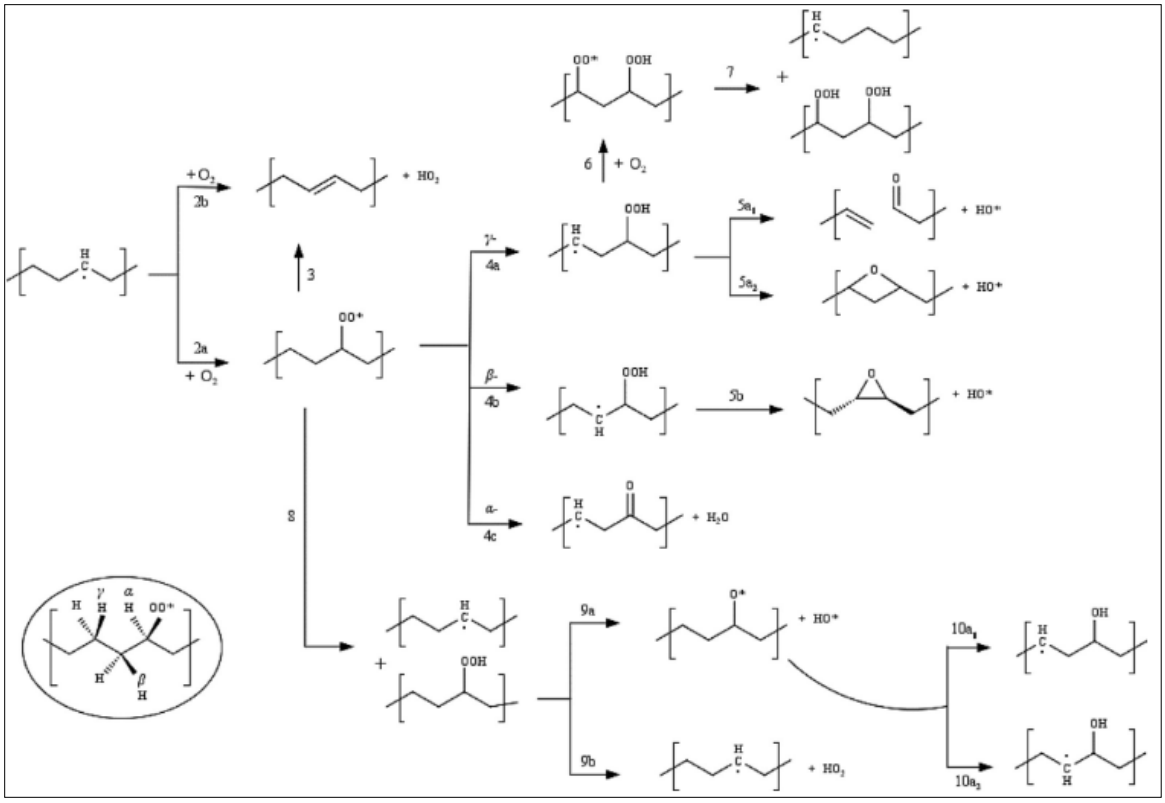

Fig 5.9: Reaction consideration of polyethylene using the radical site RO_2^* and the stereochemistry of the neighboring hydrogen atoms [62].

Figure 5.9 shows a more detailed pathways possible for the oxidation to take place by assigning hydrogens near the radical site RO_2^* in order to abstract from. Seen in

pathway 2a, the peroxy is formed via the initiation phase to form a radical. The peroxy radical can take on a few pathways specifically 4a-c and 8. Looking at the far-right side shows the final products that can be formed. Pathways 4a-c show that complex oxygen bonded products, that were not mentioned before, such as alkenes, aldehydes, 4-member ring containing a single oxygen atom, ketones as described previously, and epoxides. This also the additional contribution to the bands observed in the FTIR spectra. Following pathway 8 as a result of decomposition that results in alkoxy and alkyl radicals which result in final products with hydroxide functional group after a hydrogen abstraction. Carboxylic acid (RCOOH) yields from reaction pathway 7 where the peroxy product in the previous pathway 6 abstracts a hydrogen atom which could be Norrish II mechanism from an ester group [26].

5.5 Thermogravimetric Analysis (TGA) in Oxidative Environment

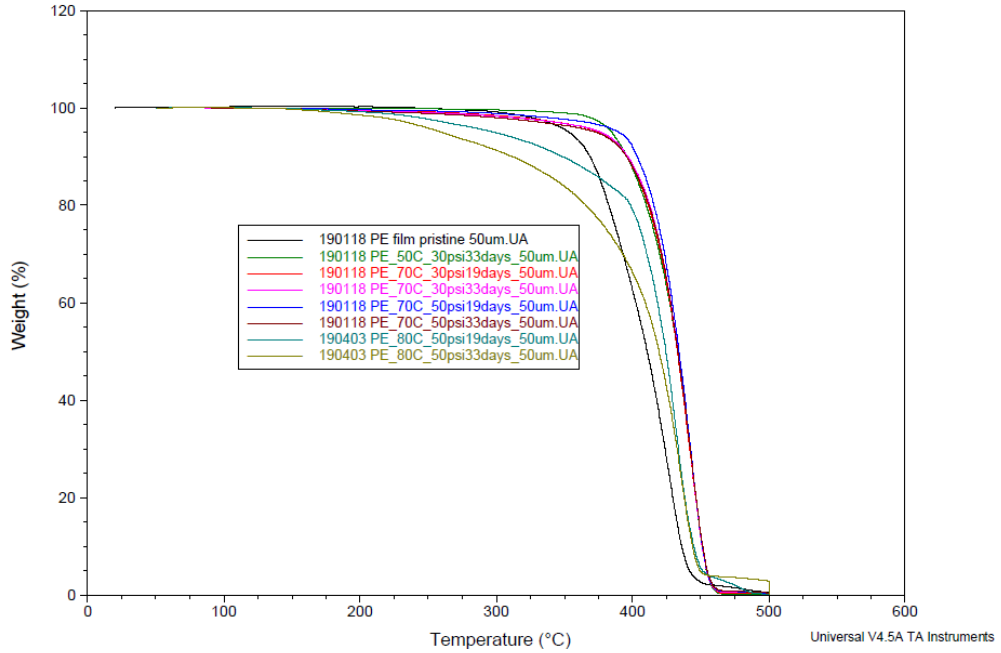

Fig 5.10: TGA curves showing the LDPE films resistance to oxidative environment after aged in the Parr vessel.

Table 5.2: TGA plot values obtained from fig 5.10 from above for comparison with pristine and aged LDPE.

				Temp (°C) @ wt%				
experimental condition	Temp (°C)	O_2 pressure (psig)	Ageing (days)	10%	50%	90%	Max Derivative Peak d(wt%)/dT)	Onset Point Temp (°C)
Pristine	-	-	0	436	411	369	427	382
Aged	50	30	33	451	433	396	443	413
Aged	70	30	19	451	433	396	442	411
Aged	70	30	33	451	433	396	443	413
Aged	70	50	19	451	434	403	443	414
Aged	70	50	33	451	433	396	443	412
Aged	80	50	19	445	424	348	434	403
Aged	80	50	33	444	419	312	433	396

Figure 5.10 and table 5.2 show the weight loss with increase in temperature which was done to see if thermal degradation and further oxidation aging lead to more dramatic weight loss. In table 5.2, max derivative peak is defined as the temperature is which the curve is steepest and onset temperature is defined as temperature where there is a transition in the weight loss has occurred. Up to 70°C, both values increase, but once the aging reaches 80°C, it decreases. Looking at temperature at 10, 50, and 90% weight loss, these represent the temperature at which the weight on that percentage of the original weight. At each percentage weight, the temperature values increase up till 70°C and then decrease at 80°C. It is important to note that values at 80°C, 50psi oxygen are greater than the pristine LDPE. From this, it shows that the stability of the aged films decreases due to the thermal degradation of the PE polymer chains as they are conforming, and bonds being broken to form oxidative products. At temperatures greater than 250°C, majority of the volatiles and lower molecular weight chains are being degraded and lost from the film. As a result, this makes it more prone to oxidative attack in the TGA apparatus. Also, in Figure 5.10, the shape of the curves can give the nature of the weight loss. At temperatures up to 70°C, the curves are similar up to 400°C, but at 80°C there is a large sharp decrease which would indicate a secondary step of degradation and oxidation process.

5.6 Mechanical Properties

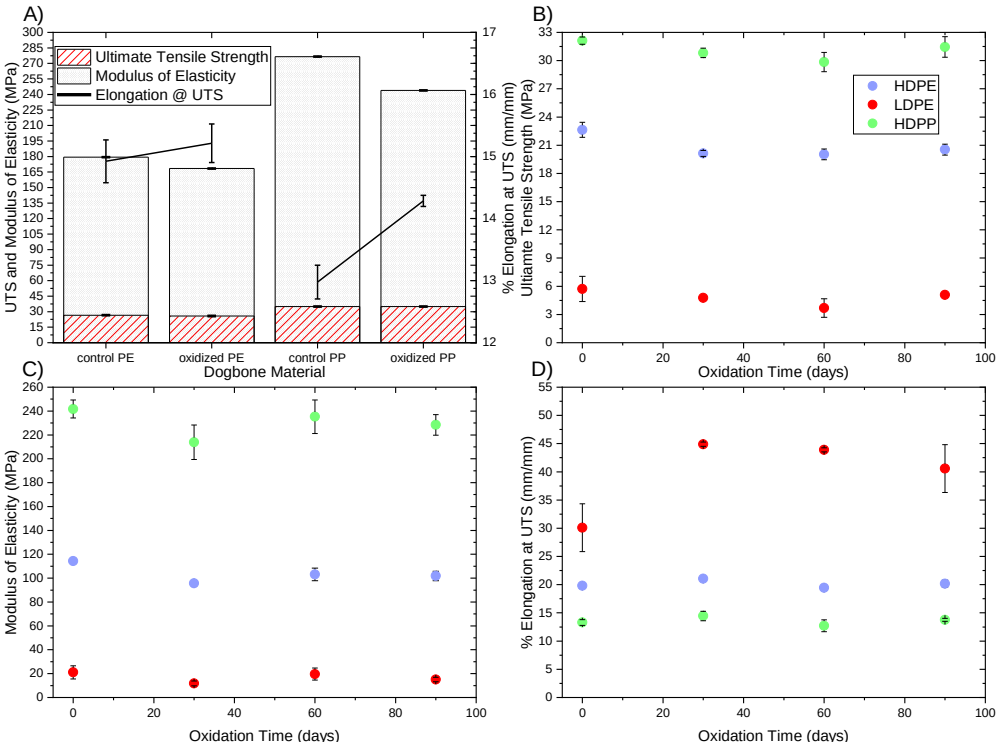

Fig 5.11: A) Ultimate Tensile Strength (UTS) and Modulus of Elasticity up to UTS plotted for ACME plastic sheet material Protec PP and Hitec HDPE aged in the Parr vessel in thermal oxidation environment for 60 days. Also, plotted is the % elongation that corresponds to the UTS value. B) UTS plotted against amount of time oxidized in Parr vessel. Legend in fig 5.11B apply to plots 5.11C and 5.11D. Plotted also are the C) Modulus of Elasticity and D) % Elongation at UTS. All dogbones have been aged in Parr vessel at 70°C and 30 psi oxygen pressure.

Figure 5.11A plots the UTS, Modulus of Elasticity, and % elongation at the UTS which are typically reported in literature and in ASTM D638−14. It shows that after 60 days of thermal oxidation of the PE in the Parr vessel, the UTS and modulus of elasticity decreased while the % elongation increased using 95% confidence (p=0.036). Since the mechanical properties were not recorded at additional times of thermal oxidation, it is difficult to see a trend at long times or it is possible the trend was missed as it may have happened in between the 60 days. From what data is present, the decrease looks to agree for the UTS and Modulus of Elasticity to previous literature even though the geometry were films unlike the dogbones in this study [52,54]. Elongation at break is often reported instead of elongation at UTS, so therefore is it likely the trend is the opposite at the UTS. This shows that at this temperature, the PE chains are relaxing and as a result the PE in

losing its mechanical strength. The % elongation at UTS, on the other hand, experienced the opposite trend as it increased as opposed to % elongation at break decreasing as seen in literature [52,54]. It is possible that it would take longer thermal oxidation times to see a decrease and the dogbones becoming brittle in nature compared to pristine PE. The same explanation could be said for the PP dogbones. For PP, the UTS and the % elongation increased while the modulus of elasticity decreased using 95% confidence ($p = 0.006$). Because of the difference in the polymer backbone, the temperature causes the crystalline structure to change so that there is mechanical degradation[53]. This is even seen in EPR, which is one of the insulative materials used in medium voltage cables [55]. K.T. Gillen, *et al.*, have attributed this to an induction time which is the time required to have an abrupt degradation in the material [55]. It is possible that longer induction time is needed to experience drastic degradation and could be explained by the antioxidants present in both sheet materials have not been completely consumed[53,55]. This can be seen in Figure 5.12, which shows a comparison picture of pristine versus thermal oxidized PE and PP dogbones. Especially in Figure 5.12B the yellowing of the PP is the indication of chemical change when the oxygen gas and antioxidants present interact with one another. This effect is not as apparent with the PE dogbone as seen in Figure 5.12A.

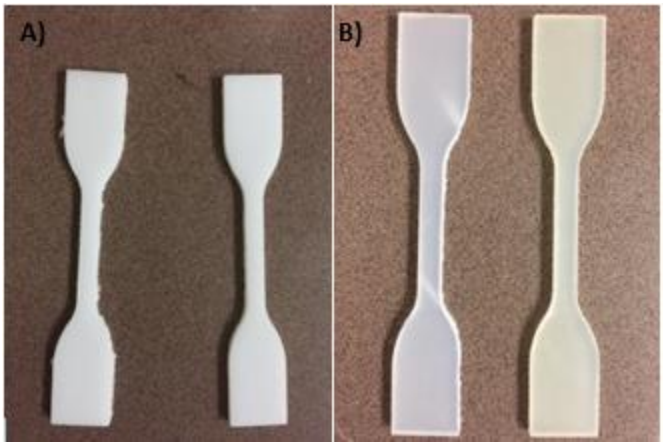

Fig 5.12: Pictures taken of the ACME plastic sheet material Protec PP and Hitec HDPE aged in the Parr vessel for 60 days at 70°C and 30 psi oxygen pressure where fig 5.12A is the HDPE and fig 5.12B is the PP. In each fig the left dogbone is pristine and the right is the aged dogbone.

Figures 5.11B through 5.11D show the UTS, Modulus of Elasticity and % Elongation at UTS for injection molded LDPE, HDPE, and HDPP dogbones. Since

dogbones were pulled out of the Parr vessel more often than in Figure 5.11A, more data points can be plotted and give a better trend of each mechanical property. It can be observed that with increasing oxidation time that the UTS and Modulus of Elasticity initially decrease and then it increases slightly and levels off. For elongation, it initially increases and then decreases and levels off [55]. Both of these changes occur at 30 days. This could be explained similarly as with Figure 5.11A, as increasing the temperature causes the chains to be more mobile and changes in crystallinity. This in turn causes the dogbone material to respond to the temperature by more favorable arrangement of the molecular chains when the sample is being pulled in the tensile tester. The initial response from the material occurs and then at longer oxidation times the material changes whether it is an increase of decrease because the chains have found the favorable conformation [55]. The initial change after 1 month increased significantly, and then leveled off after 3 months of aging and was well within error [53,55]. Comparing each material, LDPE has the smallest UTS and Modulus of Elasticity but the largest % elongation. On the other hand, HDPP had the largest UTS and Modulus of Elasticity but the smallest % elongation. This can be explained by their molecular chain composition as LDPE is composed of all hydrocarbon atoms which HDPP have a $-CH_3$ group in its chains. This causes the HDPP to have better mechanical strength, but it lacks ductility as seen in Figure 5.11D with the smaller % elongations. LDPE and HDPE, differ in that the HDPE chains are arranged in an orderly way so that the chains are packed tightly together giving rise to its larger crystalline structure as opposed to LDPE where it has more branched chains off the main chain, which result in less packed structure and less crystallinity. This explains for the larger UTS and Modulus of Elasticity of HDPE by 4-7 times but smaller % elongation than LDPE by 1.5-2 times. A physical inspection of the dogbones at each oxidation time, it did not look that there was any color change such as yellowing, and this would be expected because the dogbones were made by injection molding via pellets thus no antioxidants would be present in the melt as it was being formed in the mold. Figure 5.13 shows the dogbones at 30,60, and 90 days of aging.

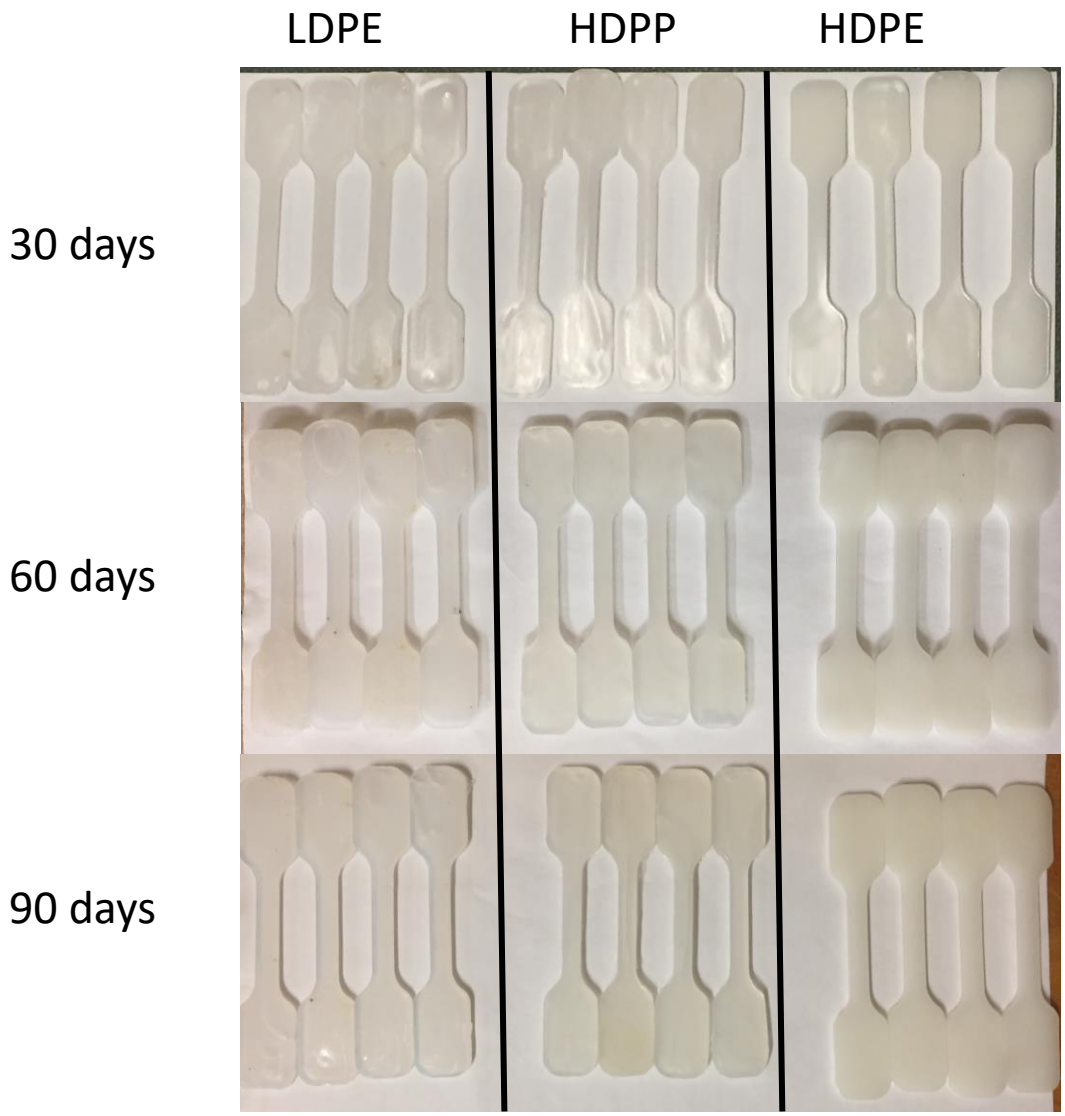

Fig 5.13: Pictures of aged dogbones taken during 70°C and 30 psi oxygen pressure in Parr vessel. The oxidation aging duration goes downward where the top row is 30 days, middle row 60 days, and finally bottom row is 90 days.

CHAPTER 6

6.1 Conclusion

Thermal oxidation and immersion of LDPE thin films was done using a Parr vessel and the extent of oxidation was monitored using the carbonyl index, a ratio quantifying the carbonyl functionality produced on the LDPE film surface. The main functional groups present were the O-H group, the carbonyl groups associated with ketones, carboxylic acids and esters. It was found that increasing the temperature, oxidation time, and oxygen pressure, increased the water-vapor permeability and the carbonyl content. The oxygen-gas only condition was compared to the WGO and ADO films at 80°C and 50 psi oxygen gas. The ADO films resulted in larger absorbance for the O-H group, the carbonyl groups associated with ketones, carboxylic acids and esters due to the more overlap in the bands. Specifically, the ADO films run for 33 days, are predicted to have the largest permeability due to it having the largest carbonyl index. The carbonyl index for the ADO films were the largest followed by the WGO films. The pH of the water decreased relative to D.I. water indicating immersed films produced highly acidic conditions as a result of the oxidation. Along with this the activation energy for the process decreased.

The results from the ATR-FTIR spectrum were analyzed and the functionality of the products were confirmed by previous work that has illustrated the reaction pathways. The TGA results confirmed that there is indeed an initial weight loss of the smaller molecular weight molecules and volatiles. At higher temperatures, there is a secondary mass loss. Up to 70°C, the mass loss curves were similar until 80°C, when the aged films decreased at a much greater rate with respect to increasing temperature. This was seen in the 10, 50, 90% weight loss temperatures. The mechanical properties of sheet PP and HDPE as well as injection molded LDPE, HDPE, HDPP dogbones were plotted with respect to the time spent in the Parr vessel during thermal oxidation. For the sheet PP and HDPE, the UTS and the modulus of elasticity decreased while the elongation increased. The injection molded LDPE, HDPE, and HDPP dogbones experienced a similar trend where the changes in the properties were within experimental uncertainty. This analysis of LDPE in dry and immersive oxygen-rich environments is an important baseline for future experiments looking at other degradation mechanisms.

6.2 Future Works

The highest temperature used was 80°C, chosen so that the film would not soften significantly or melt, otherwise it would not be feasible to test the films in the permeation cup because the films would rip. It would be beneficial and complete if the same oxidation study was done for additional temperatures above 80°C up to just below the melting point, which would be ~110°C. Along these lines, subjecting the films under higher oxygen pressures would contribute to greater oxidation and executing the experiments for multiple durations would lead to the development of better relationships. Also, as stated regarding polymers, there are antioxidants that are formulated to have desired properties. It would be beneficial to study how the antioxidants are affected with respect to the thermal oxidation. Characterizing the structure of the antioxidants would give good idea as to how it is interreacting with the polymer.

With this additional experimentation, there comes challenges with it. One of them is the analysis for activation energy for the thermal oxidation, in that the reaction mechanisms may not be the same at higher temperatures. As a result, certain steps in the reaction mechanism may become dominant at higher temperatures or vice versa. Therefore, the Arrhenius relationship will lead of different activation energies if additional mechanisms come into play.

A sample diffusion coefficient calculation was done in Appendix B using literature values to determine the solubility value of water for a given oxygen content of polyethylene. Then, from that solubility value and the permeability, the diffusion coefficient can be determined. Its inaccuracies are discussed but treating the solubility as a concentration can provide insight into how to experimentally determine it. Developing experimental procedures for water solubility that can be used on the variously aged polymer films can help in determining the diffusion coefficient and its trends with the degrees of oxidation using the Parr vessel.

Another area for further work is to determine the cross-sectional profile of the oxidation at larger depths in the polymer films and dogbones. The ATR-FTIR analysis currently is mostly a surface level analysis, it only gives insight at the level of oxidation at ~1μm depth scale. With the concern of predicting phenomenon associated with medium voltage cables such as water treeing which propagates through the insulation

material in the direction of the depth, it is important to know how the oxidation and moisture throughout the polymer film and insulation material. This would provide another level of quantitative information and would provide a better representation of the real conditions experienced by the power cables. The analysis on the percent crystallinity needs to be done as it is well established that the fraction of amorphous phase effects the behavior whether it is mechanical or chemical functionality of the polymer. Expanding the analysis for polymers with different crystalline fractions would be of the best benefit. Concurrently with this work, an IR method has been used to provide measures of the crystallinity of various polyethylene samples (Zoltec, 2019). The most common tool for determining bulk crystallinity of polymer is to use Differential Scanning Calorimetry (DSC). Also, density measurements have been frequently found to have good correlation with crystalline fraction [32].

From the last part of the results from the immersion studies done at 80°C from the WGO and ADO films, there is a lot of room for additional experiments in raising the temperature while oxygen pressure is constant inside the Parr vessel. It has been shown in the literature, that immersed and cyclic experiments result in the most degradation. A promising experiment is to increase the temperature greater than 100°C while the vessel is filled with water and oxygen gas. This allows for an increase of the vessel temperature without the water inside boiling (B.P.=100°C at 1atm). Along the lines of the antioxidants, it may be possible to leech the antioxidants out in the water that could be analyzed further. A comparison with unaged films with aged filmed under water and oxygen could be done. Appropriate aging durations would have to be used in order to have good samples for testing. Dogbones would also be incorporated to see their degradation in mechanical properties.

Because the Parr is closed vessel, extreme conditions can be employed that could not be used in a regular oven at elevated temperature. An avenue that can be explored is to try and mimic immersion conditions that would be present in a Nuclear Power Plants and those environments could be acid rain, or water with specific ions in it. This way many weathering conditions can be compared in addition to the water that was used for the preliminary immersion study in this thesis.

Also, in the context of NPPs, many literature have discussed additional polymers that are used for the insulated layers as well as jacketing layers [1]. One such example is chlorinated polyethylene (CPE), which has flame retardant properties. Running similar experiments to mimic such conditions would add to the current level of understanding of the response to environmental conditions that have been done with LDPE. It would expand the understanding from LDPE. Also, acquiring real-time samples and doing the appropriate chemical, mechanical, and electrical property testing would give us some comparison to the experimental results.

REFERENCES

[1] Busby, J. T., P. G. Oberson, C. E. Carpenter, and M. Srinivasan. 2013. “Expanded Materials Degradation Assessment (EMDA) Volume 5 : Aging of Cables and Cable Systems.” Vol. 5.

[2] Gillen, Kenneth T, and Robert Bernstein. 2010. “Review of Nuclear Power Plant Safety Cable Aging Studies with Recommendations for Improved Approaches and for Future Work.”

[3] JNES, The Final Report of the Project of “Assessment of Cable Aging for Nuclear Power Plants,” Report SS-0903, The Japan Nuclear Energy Safety Organization, 2003.

[4] Celina, M., K. T. Gillen, and R. L. Clough. "Inverse temperature and annealing phenomena during degradation of crosslinked polyolefins." Polymer degradation and stability 61, no. 2 (1998): 231-244.

[5] International Atomic Energy Agency. 2012. “Radiation Damage to Organic Materials in Nuclear Reactors and Radiation Environments.” Radiation Damage to Organic Materials in Nuclear Reactors and Radiation Environments, no. July 1989: 1. doi:IAE-TECDOC-551.

[6] Boguski, J., G. Przybytniak, and K. Łyczko. 2014. “New Monitoring by Thermogravimetry for Radiation Degradation of EVA.” Radiation Physics and Chemistry 100 (July): 49–53. doi:10.1016/j.radphyschem.2014.03.028.

[7] Seguchi, Tadao, Kazuo Arakawa, Naohiro Hayakawa, Yuhei Watanabe, and Isamu Kuriyama. "Radiation induced oxidative degradation of polymers—II." Radiation Physics and Chemistry (1977) 19, no. 4 (1982): 321-27.

[8] Seguchi, Tadao, Kiyotoshi Tamura, Takeshi Ohshima, Akihiko Shimada, and Hisaaki Kudoh. "Degradation mechanisms of cable insulation materials during radiation–thermal ageing in radiation environment." Radiation Physics and Chemistry 80, no. 2 (2011): 268-73.

[9] Villaran, M., R. Lofaro, E. Grove, and P. Soo. "Specification for Sample Preparation for Qualification Testing of Coatings to be Used in Nuclear Power Plants." Evaluation of Aging and Environmental Qualification Practices for Power Cables Used in Nuclear Power Plants, January 2003.

[10] F. Guerout L. Cisse, and R. Boor, “New Non-Destructive Condition Monitoring Techniques for On-Site Assessment of Low-Voltage Cables,” pp. 61–70 in Volume 1 of Proceedings of the ICONE 17 Conference, Brussels, Belgium, July 12–16, 2009, American Society of Mechanical Engineers, 2009

[11] Fuse, N., H. Misaka, H. Homma, and T. Okamoto. 2016. “Mechanism Elucidation of Degradation Dynamics of Ethylene Propylene Rubber Cable Insulations Sampled from Nuclear Power Containment Using Additional Aging.” IEEE Transactions on Dielectrics and Electrical Insulation 23 (2). Institute of Electrical and Electronics Engineers Inc.: 730–37. doi:10.1109/TDEI.2015.005472.

[12] Assink, Roger Alan, Kenneth Todd Gillen, and Robert Bernstein. "Nuclear Energy Plant Optimization (NEPO) final report on aging and condition monitoring of low-voltage cable materials." 2005. doi:10.2172/875986.

[13] Cao, Linfeng, and Stanislaw Grzybowski. "Accelerated aging study on 15 kV XLPE and EPR cables insulation caused by switching impulses." IEEE Transactions on Dielectrics and Electrical Insulation 22, no. 5 (2015): 2809-817. doi:10.1109/tdei.2015.004438.

[14] "Diagnosis of Medium Voltage Cables for Nuclear Power Plant." Journal of Electrical Engineering and Technology 9, no. 4 (2014): 1369-374.

[15] Lindsay, Peter, and Steve Benson. "Aging Management of Cable in Nuclear Generating Solutions." Edited by Robert K. Black. September 2012.

[16] Bahder, G., G.s. Eager, R. Suarez, S.m. Chalmers, W.h. Jones, and W.h. Mangrum. "In service evaluation of polyethylene and crosslinked polyethylene insulated power

cables rated 15 to 35 kV." IEEE Transactions on Power Apparatus and Systems 96, no. 6 (1977): 1754-766. doi:10.1109/t-pas.1977.32507.

[17] Villaran, M., R. Lofaro, E. Grove, and P. Soo. "Evaluation of Aging and Environmental Qualification Practices for Power Cables Used in Nuclear Power Plants." Evaluation of Aging and Environmental Qualification Practices for Power Cables Used in Nuclear Power Plants, January 2003.

[18] Jacobus, Mark J. “Loss-of-Coolant Accident (LOCA) Testing of Aged Cables with Application to Nuclear Plant Life Extension.” *Nuclear Engineering and Design*, vol. 134, no. 2-3, 1992, pp. 267–275., doi:10.1016/0029-5493(92)90144-k.

[19] Lofaro, R., et al. “Assessment of Environmental Qualification Practices and Condition Monitoring Techniques for Low-Voltage Electric Cables: LOCA Test Results.” *Assessment of Environmental Qualification Practices and Condition Monitoring Techniques for Low-Voltage Electric Cables*, Jan. 2001, doi:10.2172/1329393.

[20] Paul M. Bhadha, "How Weld Hose Materials Affect Shielding Gas Quality", AWS Welding Journal, pp. 35-37, Jul. 1999.

[21] Lin, Y.J., et al. “Oxygen Permeability of Biaxially Oriented Polypropylene Films.” Polymer Engineering &Amp; Science, vol. 48, no. 4, 2008, pp. 642–648.

[22] Rubino, Maria, Marvin A. Tung, Sylvia Yada, and Ian J. Britt. "Permeation of Oxygen, Water Vapor, and Limonene through Printed and Unprinted Biaxially Oriented Polypropylene Films." *Journal of Agricultural and Food Chemistry*49, no. 6 (2001): 3041-045. doi:10.1021/jf001427s.

[23] Wichterlová, Jana, Kamil Wichterle, and Jiří Michálek. "Determination of Permeability and Diffusivity of Oxygen in Polymers by Polarographic Method with Inert Gas." *Polymer*46, no. 23 (2005): 9974-986. doi:10.1016/j.polymer.2005.06.125.

[24] Paterson, Russell, Yuri Yampol'Skii, Peter G. T. Fogg, Alexandre Bokarev, Valerii Bondar, Oleg Ilinich, and Sergey Shishatskii. "IUPAC-NIST Solubility Data Series 70. Solubility of Gases in Glassy Polymers." *Journal of Physical and Chemical Reference Data*28, no. 5 (1999): 1255-450. doi:10.1063/1.556050.

[25] Tung, Kevin K., R.t. Bonnecaze, B.d. Freeman, and D.r. Paul. "Characterization of the Oxygen Scavenging Capacity and Kinetics of SBS Films." *Polymer*53, no. 19 (2012): 4211-221. doi:10.1016/j.polymer.2012.07.028.

[26] Chabira, Salem F., Mohamed Sebaa, and Christian Gsell. "Oxidation and Crosslinking Processes during Thermal Aging of Low-density Polyethylene Films." *Journal of Applied Polymer Science*, December 14, 2011. doi:10.1002/app.34080.

[27] Reddy, Murali Mohan, Margaret Deighton, Satinath Bhattacharya, and Rajarathinam Parthasarathy. "Biodegradation of Oxo-biodegradable Polyethylene." *Journal of Applied Polymer Science*113, no. 5 (2009): 2826-832. doi:10.1002/app.30327.

[28] Hakkarainen, Minna, and Ann-Christine Albertsson. "Environmental Degradation of Polyethylene." *Long Term Properties of Polyolefins Advances in Polymer Science*: 177-200. doi:10.1007/b13523.

[29] Coote, Christopher F., John V. Hamilton, W. Grant Mcgimpsey, and Robert W. Thompson. "Oxidation of Gamma-irradiated Ultrahigh Molecular Weight Polyethylene." *Journal of Applied Polymer Science*77, no. 11 (January 26, 2000): 2525-542. doi:10.1002/1097-4628(20000912)77:113.0.co;2-i.

[30] Oluwoye, Ibukun, Mohammednoor Altarawneh, Jeff Gore, Henning Bockhorn, and Bogdan Z. Dlugogorski. "Oxidation of Polyethylene under Corrosive NOx Atmosphere." *The Journal of Physical Chemistry C*120, no. 7 (2016): 3766-775. doi:10.1021/acs.jpcc.5b10466.

[31] Siracusa, Valentina. “ Food Packaging Permeability Behavior: A Report.” *International Journal of Polymer Science2012* (February 16,2012): 1−11. doi:10.1155/2012/302029

[32] Michaels, Alan S., and Harris J. Bixler. “ Flow of Gases through Polyethylene.” *Journal of Polymer Science*50, no. 154 (1961): 413-39. doi: 10.1002/pol.1961.1205015412

[33] Michaels, Alan S., and R.B. Parker. “ Sorption and Flow of Gases through Polyethylene.” *Journal of Polymer Science*41, no. 138 (1959): 53-71 doi: 10.1002/pol.1959.1204113805

[34] Mrkić, Saša, Kata Galić, Marica Ivanković, Sandra Hamin, and Nada Ciković. "Gas Transport and Thermal Characterization of Mono- and Di-polyethylene Films Used for Food Packaging." *Journal of Applied Polymer Science*99, no. 4 (June 24, 2005): 1590-599. doi:10.1002/app.22513.

[35] Peacock, Andrew, and Marcel Dekker. "Handbook of Polyethylene: Structures, Properties, and Applications." 2000. doi:10.1201/9781482295467.

[36] Tipnis, Namita P., and Diane J. Burgess. "Sterilization of Implantable Polymer-based Medical Devices: A Review." *International Journal of Pharmaceutics*544, no. 2 (2018): 455-60. doi:10.1016/j.ijpharm.2017.12.003.

[37] Kurtz, Steven M. *Uhmwpe Biomaterials Handbook Ultra-high Molecular Weight Polyethylene in Total Joint Replacement and Medical Devices*. Amsterdam: William Andrew, an Imprint of Elsevier, 2016.

[38] Hiemenz, Paul C., and Timothy Lodge. *Polymer Chemistry*. 2nd ed. Boca Raton: CRC Press, 2007.

[39] Pauly, S. "Permeability and Diffusion Data." The Wiley Database of Polymer Properties, 2003. doi:10.1002/0471532053.bra045.

[40] Tetens, O. 1930. Uber einige meteorologische Begriffe. z. Geophys.6:297-309.

[41] Shibryaeva, Lyudmila. 2012. “Thermal Oxidation of Polypropylene and Modified Polypropylene - Structure Effects.” Polypropylene, 63–86. doi:10.5772/2229.

[42] Iring, M, and F. Tüdös. 1990. “Thermal Oxidation of Polyethylene and Polypropylene: Effects of Chemical Structure and Reaction Conditions on the Oxidation Process.” Progress in Polymer Science 15 (2): 217–62. doi:10.1016/0079-6700(90)90029-Z.

[43] Peterson, Jeffery D., Sergey Vyazovkin, and Charles A. Wight. 2001. “Kinetics of the Thermal and Thermo-Oxidative Degradation of Polystyrene, Polyethylene and Poly(Propylene).” Macromolecular Chemistry and Physics 202 (6): 775–84. doi:10.1002/1521- 3935(20010301)202:6<775::AID-MACP775>3.0.CO;2-G.

[44] "Home." Corrosion Control Publications. Accessed December 04, 2018. https://www.dipra.org/ductile-iron-pipe-resources/technical-publications/corrosion-control.

[45] Myers, A. W., J. A. Meyer, C. E. Rogers, V. Stannett, and M. Szwarc. "The Gas and Vapor Permeability of Plastic Films and Coated Papers. VI. The Permeation of Water Vapor." *Technical Association of the Pulp and Paper Industry ©1949*-44, no. 1 (January 1961): 58-64.

[46] Fox, Charles J. J. "On the Coefficients of Absorption of Nitrogen and Oxygen in Distilled Water and Sea-water, and of Atmospheric Carbonic Acid in Sea-water." *Transactions of the Faraday Society*5, no. September (April 27, 1909): 68. doi:10.1039/tf9090500068.

[47] Shchukarev, S. A., and T. A. Tolmacheva. "Solubility of Oxygen in Ethanol ? Water Mixtures." *Journal of Structural Chemistry*9, no. 1 (June 15, 1968): 16-21. doi:10.1007/bf00744018.

[48] Wise, D.l., and G. Houghton. "Solubilities and Diffusivities of Oxygen in Hemolyzed Human Blood Solutions." *Biophysical Journal*9, no. 1 (June 5, 1968): 36-53. doi:10.1016/s0006-3495(69)86367-8.

[49] Pray, H. A., Stephan, Elmer F, Battelle Memorial Institute, and U.S. Atomic Energy Commission. *The Solubility of Hydrogen in Uranyl Sulphate Solutions at Elevated Temperatures*. U.S. Atomic Energy Commission, Technical Information Service, 1955.

[50] Pray, H. A. H, Peoples, Robert S, Hatfield, Nathan S, Stephan, Elmer F, Battelle Memorial Institute, and U.S. Atomic Energy Commission. *The Solubility of Gases in Water and in Aqueous Uranyl Salt Solutions at Elevated Temperatures and Pressures*. Battelle Memorial Institute, 1956.

[51] Pray, H. A., C. E. Schweickert, and B. H. Minnich. "Solubility of Hydrogen, Oxygen, Nitrogen, and Helium in Water at Elevated Temperatures." *Industrial & Engineering Chemistry*44, no. 5 (December 31, 1951): 1146−151. doi:10.1021/ie50509a058.

[52] Suresh, Balasubramanian, S. Maruthamuthu, Alika Khare, N. Palanisamy, V. S. Muralidharan, R. Ragunathan, M. Kannan, and K. Navaneetha Pandiyaraj. "Influence of Thermal Oxidation on Surface and Thermo-mechanical Properties of Polyethylene." *Journal of Polymer Research* 18, no. 6 (2011): 2175−184. doi:10.1007/s10965-011-9628-0.

[53] Gillen, K.t., R. Bernstein, R.l. Clough, and M. Celina. "Lifetime Predictions for Semi-crystalline Cable Insulation Materials: I. Mechanical Properties and Oxygen Consumption Measurements on EPR Materials." *Polymer Degradation and Stability*91, no. 9 (January 18, 2006): 2146−156. doi:10.1016/j.polymdegradstab.2006.01.009.

[54] Jeon, Hyun Jeong, and Mal Nam Kim. "Degradation of Linear Low Density Polyethylene (LLDPE) Exposed to UV-irradiation." *European Polymer Journal*52 (January 7, 2014): 146-53. doi:10.1016/j.eurpolymj.2014.01.007.

[55] Gonokami, M., Y. Ohtake, and S. Kawahara. "Dissolution Behaviour of the Antioxidant in Polypropylene in Tap Water and Evaluation of the Polymer Degradation." *International Polymer Science and Technology*38, no. 12 (November 9, 2011): 53-59. doi:10.1177/0307174x1103801212.

[56] Wise, J., K.t. Gillen, and R.l. Clough. "Quantitative Model for the Time Development of Diffusion-limited Oxidation Profiles." *Polymer*38, no. 8 (June 17, 1997): 1929-944. doi:10.1016/s0032-3861(96)00716−1.

[57] Sastry, P. Krishna, D. Satyanarayana, and D. V. Mohan Rao. "Accelerated and Environmental Weathering Studies on Polyethylene-starch Blend Films." *Journal of Applied Polymer Science*70, no. 11 (1998): 2251-257. doi:10.1002/(sici)1097-4628(19981212)70:113.0.co;2−1.

[58] Luongo, J. P. "Infrared Study of Oxygenated Groups Formed in Polyethylene during Oxidation." *Journal of Polymer Science*42, no. 139 (1960): 139-50. doi:10.1002/pol.1960.1204213916

[59] Iring, M., and F. Tudos. "Thermal Oxidation of Polyethylene and Polypropylene: Effects of Chemical Structure and Reaction Conditions on the Oxidation Process." *Progress in Polymer Science*15, no. 2 (1990): 217-62. doi:10.1016/0079-6700(90)90029-z.

[60] Mccall, D. W., Dean C. Douglass, L. L. Blyler, G. E. Johnson, Lynn W. Jelinski, and H. E. Bair. "Solubility and Diffusion of Water in Low-density Polyethylene." *Macromolecules*17, no. 9 (1984): 1644-649. doi:10.1021/ma00139a001.

[61] Geng, Ming, and Zhenhao Duan. "Prediction of Oxygen Solubility in Pure Water and Brines up to High Temperatures and Pressures." *Geochimica Et Cosmochimica Acta*74, no. 19 (June 28, 2010): 5631-640. doi:10.1016/j.gca.2010.06.034.

[62] Oluwoye, Ibukun, Mohammednoor Altarawneh, Jeff Gore, and Bogdan Z. Dlugogorski. "Oxidation of Crystalline Polyethylene." *Combustion and Flame*162, no. 10 (July 2, 2015): 3681-690. doi:10.1016/j.combustflame.2015.07.007.

[63] Zoltek, Daniel T. “Developing a Predictive Model and Novel Imaging Technique for the Failure of Polyethylene Insulators” Master’s Thesis., University of Minnesota Duluth, 2019

APPENDICIES

Appendix A : Controlling and Monitoring the Temperature of Thermal Oxidation

In this thesis work, it was very important that the temperature was controlled for an entire thermal oxidation experiment; this was achieved with the Parr 4838 temperature controller programmed for PID controller. PID stands for Proportional-Integral-Derivative control and is the common feedback algorithm used to control of a system parameter which in this case is temperature, *T*, of the Parr reactor. The P, I & D parts are combined together depending on the application to deliver the optimum control signal to obtain the desired system temperature, T_{sp}, called the set point. The signal is compared to the system parameter value and then an error is calculated which is simply the difference. The signal from the temperature sensor, $T_{pv}(t)$, is compared to the set point and then an error, $e(t)$, is calculated from the difference.

$$e(t) = T_{sp} - T_{pv}(t) \qquad (A1)$$

On the controller's display, the sensor reading is designated by "PV". The general PID control algorithm is defined by the controller output $C(t)$, a function with respect to the time, t , after the controller is switched on:

$$C(t) = C_0 + K_c\left[e(t) + \frac{1}{\tau_I}\int_0^t e(t)dt + \tau_D\frac{de(t)}{dt}\right], \qquad (A2)$$

where C_0 is the value of the controller output when it is turned on, called the bias. The bias gives rise to the desired steady-state temperature in open-loop, or manual mode (the control algorithm is off). K_c is the proportional gain; τ_I and τ_D are the integral and derivative times, respectively. These three constants are the user-selected tuning parameters. Each of the three time-dependent parts respond differently to the error. Proportional control, the term linear in the error, acts upon the current error. The integral term sums the past errors to reduce the current net error. The derivative control is responsible of estimating the future trend of the error and responds to its current rate of change

Implementation for the Parr 4838 temperature controller.

The large thermal capacity of the pressure vessel, in which the thermal oxidations were done, led to difficulties in obtaining working controller settings — the response times are long, of the order of hours. The controller has an auto tune function, but this

proved unworkable because of the large overshoots from the set point during the tuning sequence. (The controller is really designed to handle set-points much higher than the ones used here — up to 800°C.) It was determined that using the Proportional control only was the best and simplest option, even though small overshoots would occur for the gains used. The controller output function becomes:

$$C(t) = C_0 + K_c[e(t)], \tag{A3}$$

which shows that the error term is only proportional to as single user-defined tuning term. The proportional gain on the controller is set by using the related proportional band, PB:

$$PB = \frac{1}{K_c} \tag{A4}$$

In the context of this controller, the controller output function is the fraction of the maximum power capable of being delivered to the heater surrounding the pressure vessel. The controller was switched on from ambient conditions, so $C_0 = 0$, this leads to:

$$PB = \frac{e(t)}{C(t)}, \tag{A5}$$

For example, the default setting for the proportional band on the controller is 12°C. This means the error has to be 12°C for the controller to deliver its maximum power whence, $C(t) = 1$. For the most part a proportional band of 200°C was used.

The main disadvantage of P-only control is the phenomenon of offset that arises from not starting the system in open-loop mode (manual control) with a bias value that gives rise to the desired steady-state temperature. (A way has yet to be been found to do this with this controller.) However, a heuristic method was developed as a work-around. Offset means that when the set-point is changed from that corresponding to a particular bias, the final steady-state temperature, T_{ss}, will not coincide with the set point, but will be offset from it. Simple control theory leads to:

$$\text{Offset} = T_{sp} - T_{ss} = \frac{T_{sp}}{1 + K_c K_p} \tag{A6}$$

Here K_p is the steady-state process gain ($K_p = \Delta T_{pv}/\Delta C$) determined from open-loop experiments, and it is assumed to be independent of the temperature. The heuristic method is best illustrated by an example.

Example: Using a PB of 300°C for a set-point (SV on the controller display), $T_{sp} = 50°C$, a final steady-state temperature, $T_{ss} = 44°C$, was observed. This enables an estimate of $1 + K_c K_p$ to be made from eq A6 above: $1 + K_c K_p = 25/3$. Now we turn the problem around and ask what set point will give a steady state temperature of 50°C? Rearranging eq A6 gives:

$$T_{sp} = T_{ss} \times \frac{1 + K_c K_p}{K_c K_p} = 57°C$$

Finally, a set point of 59°C gave a steady-state temperature of 50°C after further trials. It is not an exact procedure as K_p is not in fact constant, but it does provide a starting point for the user running the experiment to get the desired setpoint temperature. Similar procedures were followed for other desired temperatures.

The Table below shows typical settings on the '**Press "Set" and release**' menu (lower right-hand table on p.18 of the controller manual) used for the desired temperature of 80°C.

Table A1. Parr controller entries when "Set" is pressed and release for the desired temperature of 80°C.

Operation Mode	Select type/value	Comment
At	OFF	AutoTuning ON/OFF
PID2	82°C	The 2nd set of PID parameters, identified by the set point
SV	82°C	The set point
P2	200°C	The proportional band
I2	0	Integral time, 0 means "off".
D2	0	Derivative time, 0 means "off".

Note 1: Other settings in this menu system are as in the manual.
Note 2: Heater switch setting used throughout: LOW(I) position

The measured temperature profiles on the inside of the Parr vessel after the controller is switched on are shown below in Figure A1. The small overshoots between about1½ and 2½ hours could be eliminated by using higher values of the proportional band, but the response times would be longer.

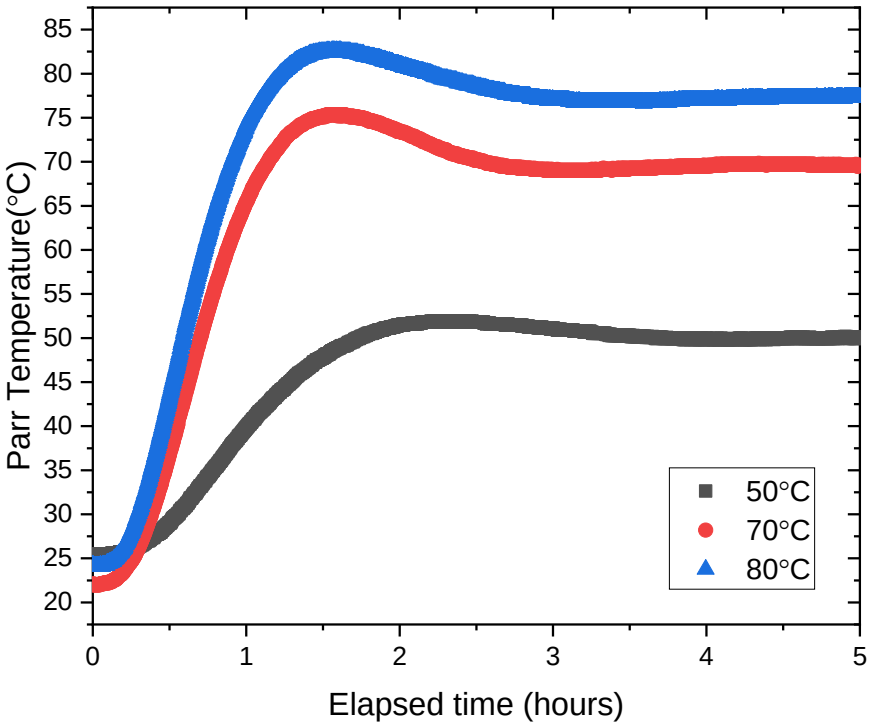

Fig A1: Plots constructed of the temperature profile of the Parr vessel at the desired "set point" temperatures of 50, 70, and 80°C using the proportional band of 200°C except for 50°C which was done at proportional band of 300°C. The oxygen pressure was at a constant 30psi.

Appendix B: Sample Calculation of Permeation using the Experimental Mass vs Time Permeation Cup Loss Data

Permeability:

As illustrated in the theory part of this thesis, the calculation of permeability eq. 2.21 & 2.23 requires the thickness of the film, the pressure gradient across the cup, and the area of the region through which the water vapor is crossing the film membrane. Fig B1 below shows the raw mass loss over time for a control of pristine and a set of three LDPE films aged at a certain temperature and oxygen pressure.

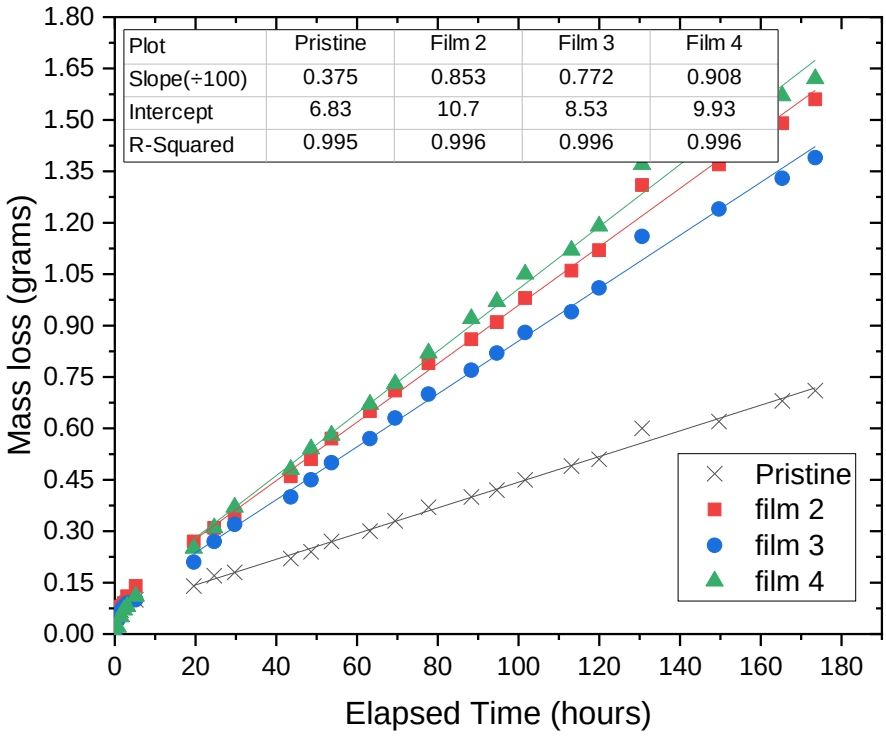

Fig B1: Permeation cup mass loss data during a run for ~ 7 days in 60°C oven. The films 2 to 4 had been in the Parr vessel at 80°C and 50psi oxygen pressure for 33 days. The slope and intercepts calculated from the best-fit line were multiplied by 100 for accuracy in significant digits.

Looking at the theory section in Chapter 2.3 and the equations, the slope of the mass loss-time lines in Figure B1 is, $\dot{m}$. This is the necessary starting point to determine the permeability which has both a concentration of water and a pressure difference with the latter being used for this calculation. The calculation for pristine LDPE is presented here as an example of the calculations will be done for the other aged films.

From Figure B1, the slope of the best-fit line steady state mass loss is:

$$slope = \dot{m} = 0.00375 \approx 0.004 \frac{g}{hr}$$

The flux of water vapor across the film, WVT using eq 2.16, converting the slope to seconds and multiply by the area of the permeation cup results in:

$$\frac{\dot{m}}{A} = 0.004 \frac{g}{hr} \times \frac{1}{3600} \frac{hr}{s} \times \frac{1}{12.25 cm^2} = 9.07 \times 10^{-8} \frac{g}{s \times cm^2}$$

We now require the change in vapor pressure, Δp_{vap}. Using the Tetens equation 2.19 for 60°C oven with ~2.8% humidity(monitored by humidity probe) and 100% saturated water vapor, the vapor pressure on each side can be calculated.

Inside the cup, assuming to be 100% saturated with water vapor at steady state, the saturated vapor pressure can be calculated as:

$$p_{sat} = 610.78 \times e^{\frac{17.2694*60}{60+238.3}} = 19698.55\ Pa$$

Outside the cup the humidity is governed by the oven. Using the 60°C oven with ~2.8% humidity conditions, the saturated vapor pressure will just be a fraction of the saturated vapor pressure:

$$p = p_{sat} \times RH = 19698.55 \times \frac{2.8}{100} = 551.56\ Pa$$

Take the difference between the two values will give the water partial pressure difference across the LDPE film:

$$\Delta p_{vap} = 19698.55 - 551.56 = 19147.0\ Pa$$

Converting the pressure to the desired units results in:

$$\Delta p_{vap} = 19146.99\ Pa \times \frac{1}{133.32} \frac{mmHg}{Pa} \times \frac{1}{10} \frac{cmHg}{mmHg} = 14.36 cmHg$$

Substituting the thickness in equation 2.21 and the water partial pressure difference terms in results in a permeability of:

$$P = \frac{9.07 \times 10^{-8} \frac{g}{s \times cm^2} \times 0.005\ cm}{14.36 cmHg} = 3.16 \times 10^{-11} \frac{g \times cm}{s \times cm^2 \times cmHg}$$

This gives the permeability under the experimental conditions (60°C, 2.8% RH) in terms of mass of water vapor. We need to covert this to the volume of water vapor under conditions of STP in order to determine the final permeability in units of Barrer shown in equation 2.23. To do this, we need the factor:

$$\frac{RT^0}{M_w P^0} = \frac{62356 cm^3 \times mmHg \times mol^{-1} \times K^{-1} \times 273.15K}{18.015g \times mol^{-1} \times 760 mmHg} = 1244.03 \frac{cm^3_{STP}}{g}$$

This factor represents the specific volume of water vapor at STP. The corresponding permeability at STP is:

$$P = 3.16 \times 10^{-11} \frac{g \times cm}{s \times cm^2 \times cmHg} \times 1244.03 \frac{cm^3_{STP}}{g} = 3.9311 \times 10^{-8} \frac{cm \times (\frac{cm^3_{STP}}{s})}{cm^2 \times cmHg} =$$

393 Barrer

The values may be more accurately determined using spreadsheets such as Excel as there was many places to round off decimal values. This was for the demonstration of how permeability is calculated using experimental values of the mass loss over time.

Along with the use of the pressure difference with Tetens equation shown above, a comparison can be done with the Ideal Gas law showing how much pressure is built-up inside the permeation cup at ambient temperatures before the experiment versus when the cups are in the oven during the experiment. The reason to look at it this way is because as the pressure is built-up in the permeation cup, it can influence the permeability as well as stretching it physically.

Taking the Ideal Gas law for a constant volume and substance, known as Guy-Lussac's Law, which is written as:

$$\frac{P_1}{T_1} = \frac{P_2}{T_2}, \qquad (B1)$$

where the subscripts 1 & 2 denote two different set of conditions and *P* and *T* are the pressure and temperature (in Kelvins) respectively.

Taking subscript 1 as ambient temperature, taken as 27°C, and subscript 2 as the oven temperature (60°C, 70°C, and 90°C) and grouping the pressure, *P*, terms in equation B1, the ratio between 27°C and the oven temperatures can be determined:

$$\frac{P_2}{P_1} = \frac{T_2}{T_1} \equiv \frac{P_{60℃}}{P_{27℃}} = \frac{T_{60℃}}{T_{27℃}} = \frac{273.15 + 60}{273.15 + 27} = 1.11 \; or \; P_{60℃} = 1.11 P_{27℃}$$

$$\frac{P_{60℃}}{P_{27℃}} = \frac{T_{70℃}}{T_{27℃}} = \frac{273.15 + 70}{273.15 + 27} = 1.14 \; or \; P_{70℃} = 1.14 P_{27℃}$$

$$\frac{P_{60℃}}{P_{27℃}} = \frac{T_{90℃}}{T_{27℃}} = \frac{273.15 + 90}{273.15 + 27} = 1.21 \; or \; P_{90℃} = 1.21 P_{27℃}$$

Appendix C: Sample Calculation of the Diffusion Coefficient using Solubility

The estimation of the diffusion constant from permeability and solubility is demonstrated with an example. From eq. 2.35:

$$D = P/S$$

The solubility is derived from the study of McCall *et al.* [60] on polyethylene and water. This is illustrative because they use "solubility" in the more usual sense – this can be deduced by the quantity's units (the absence of pressure units, in particular). The units of S are quantity per unit volume per unit pressure; the SI choice is kmol per cubic meter per bar. The units of c are then kmol per cubic meter from eq. 2.33. Their solubility is quoted in ppm, so it is a mass fraction — this means that their solubility is really a measure of the concentration c, say c'. So

$$c' = \frac{m_w}{m_w + m_s} \qquad (C1)$$

Here m_w is the mass of dissolved water in the film and m_s is the mass of the solid film. Usually, $m_s \gg m_w$ so:

$$c' = \frac{nM_w}{\rho_s V_s} = \frac{M_w}{\rho_s} c \qquad (C2)$$

Here n are moles of water; M_w is the molar mass of water; ρ_s is the density of the solid film; and, V_s is its volume.

So, concentration can now be expressed as:

$$c = \frac{\rho_s}{M_w} c' \qquad (C3)$$

For example, from Fig. 3 of McCall et al, a value of c' is 400 ppm, corresponding to

$$c = \frac{920 \text{ kg m}^{-3} \times 400 \times 10^{-6}}{18.015 \text{ kg kmol}^{-1}} = 0.0204 \text{ kmol m}^{-3}$$

using the value for the density of polyethylene of $\rho_s = 920$ kg m^{-3}. This was determined at 25 °C for polyethylene equilibrated with water. Under these conditions, $p \equiv p_{sat} = 0.03166$ bar; this leads to the corresponding solubility:

$$S = \frac{c}{P} = 0.645 \text{ kmol m}^{-3}\text{bar}^{-1}$$

The value of the permeability from Appendix B is:

$$P = 393 \text{ Barrer} = \frac{3.93 \times 10^{-8}\text{cm} \times \text{cm}^3_{STP}/\text{s}}{\text{cm}^2 \times \text{cmHg}}$$

We convert this to SI units using the following conversions:

$$1\ \mathrm{cm}^3_{STP}/\mathrm{s} \equiv \frac{(10^{-6}\ \mathrm{m}^3_{STP}/\mathrm{s})}{2.41\ \mathrm{m}^3_{STP}\mathrm{kmol}^{-1}} = 4.149 \times 10^{-7}\ \mathrm{kmol\ s}^{-1}, \text{ and } \ 1\mathrm{cmHg} \equiv 0.0133\mathrm{bar}$$

Now:

$$P = \frac{3.93 \times 10^{-8} \times 10^{-2}\mathrm{m} \times 4.149 \times 10^{-7}\ \mathrm{kmol\ s}^{-1}}{10^{-4}\mathrm{m}^2 \times 0.0133\ \mathrm{bar}} = 9.41 \times 10^{-11}\frac{\mathrm{kmol}}{\mathrm{s} \times \mathrm{m} \times \mathrm{bar}}$$

Finally:

$$D = \frac{P}{S} = \frac{9.409 \times 10^{-7}\mathrm{kmol.s}^{-1}.\mathrm{m}^{-1}.\mathrm{bar}^{-1}}{0.645\ \mathrm{kmol\ m}^{-3}\mathrm{bar}^{-1}} = 1.46 \times 10^{-10}\frac{\mathrm{m}^2}{\mathrm{s}} = 1.46 \times 10^{-6}\frac{\mathrm{cm}^2}{\mathrm{s}}$$

This is at the high end of the expected range for diffusion within solids, but it should be emphasized that data on two different samples from two different sources have used solely for purposes of this sample calculation.

Appendix D: Smoothing of the Tensile Test Data from MTS Tensile Tester

Using the MTS tensile tester at a rate of 5 mm/min, this leads to a lot of data points of the displacement and force determined each second and as a result the amount of noise in the data can be extremely bothersome. Another source of noise is in the MTS testing instrument's hydraulic system designed for metal samples. Wherever the source of noise is from, the noise results in a band of values and in order to make the values useful, a filter technique is employed in generating a clearer mean value for a small time step.

To make the data more manageable in order to determine the important mechanical properties such as the UTS and the elongation, the raw data needs to be smoothened using a filter so that there are less points but at the same time it does not ruin the integrity of the data. A Savitzky-Golay digital filtering is applied for smoothing the data, that is, to increase the precision of the data without distorting the signal tendency. This is achieved using a process called convolution, which is fitting successive groups of adjacent data points with a low-degree polynomial using linear least squares. The linear least squares can then be solved for an analytical solution in the form of a single set of "convolution coefficients" that can be applied to all data groupings, to give estimates of the smoothed signal) at the central point of each group of points.
The iterative equation can be mathematically shown for a data that consists of a set (x_j,y_j) which points (j=1,2,3…n):

$$Y_j = \sum_{i=0.5-0.5m}^{0.5m-0.5} C_i y_j\,, \qquad 0.5m - 0.5 \le j \le n - 0.5m - 0.5 \qquad (D1)$$

where *x* is the independent variable(displacement), *y* is the observed value(force), and C_i are the convolution coefficients in which there are a set of *m* coefficients. The coefficients can be found in various table. With powerful software such as MATLAB, there are user-defined functions that do the work on the data. In the case of MATLAB, the function is sgolayfilt(x,order,framelen) where the user can input the signal of concern(force) and the order of the polynomial that will be used, and then finally the amount of points used to fit to that polynomial. From this, a script can be written to take the raw data, filter it, and then finally have in terms of stress verses strain in a convenient spreadsheet.

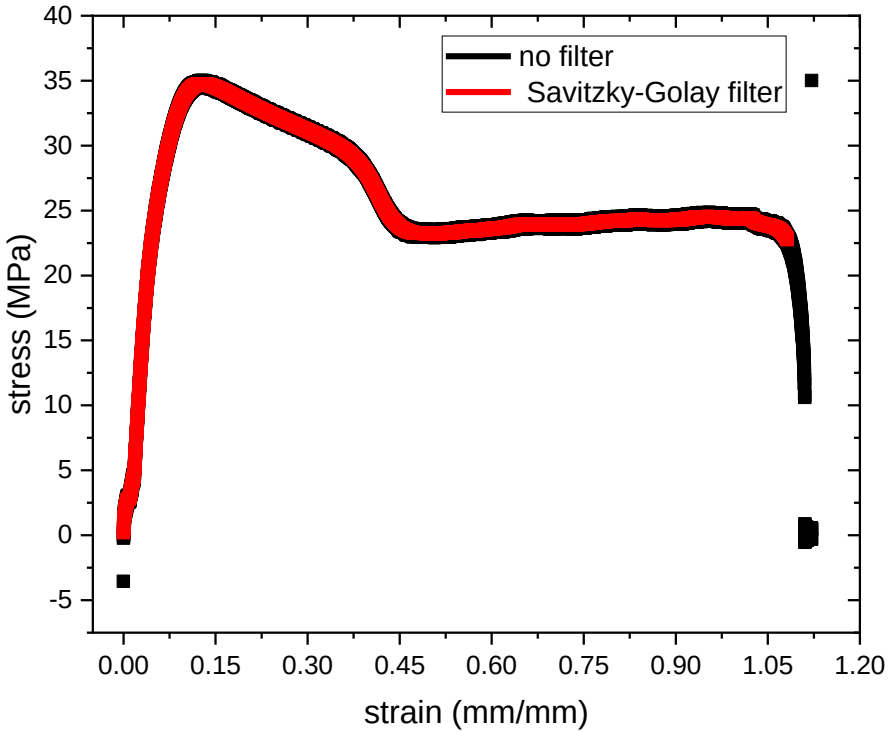

Fig D1: Plots of control Protec sheet PP stress versus strain of the raw data and the data with smoothing function applied to it. A Savitzky-Golay filtering was done using a 3rd order polynomial using 61 points for the polynomial fitting.